ORI

ORI 1400 SPRING STREET
Silver Spring, Maryland 20910

FLOW NOISE AND OUTER DECOUPLER STUDIES

3 DECEMBER 1982

PREPARED UNDER CONTRACT No. N00014-82-C-1547

PREPARED FOR:

THE OFFICE OF NAVAL RESEARCH
DEPARTMENT OF THE NAVY
800 NORTH QUINCY STREET
ARLINGTON, VIRGINIA 22217

TABLE OF CONTENTS

1.0 INTRODUCTION AND SUMMARY

As has been brought out repeatedly at the ACSAS industry briefing and at the June, 1982 workshop, a viable technique for the mitigation of low wavenumber flow-induced noise at higher submarine speeds is the most important advance that could result from the ACSAS effort. Historians, militarists and scientists all can agree that you must know your enemy before you can defeat him. Therefore, our approach in the very limited effort funded by the ACSAS program to date has been to start on the development of at least a rudimentary description of the nature of the low-wavenumber noise production mechanisms and features. We feel that we have made some progress -- the reader can make his own judgement -- and we report that progress herein.

Briefly we demonstrate that certain responses and mechanisms must be considered and included in even a minimal model of the turbulent boundary layer (TBL) low-wavenumber pressure fluctuation production processes and the attendant stipulation of outer decoupler design guidelines. Specifically, we show that to explain the observed features of the noise spectra you must include:

(1) Cyclic, self-sustaining nonlinear interactions of packets of finite-amplitude Tollmien-Schlicting waves intrinsically subject to large phase modulations.

(2) The continuous spectrum of modes of response of the TBL to Reynolds stress bursts.

3) Nonlinear interactions between the continuous spectrum modes.

The measured features of low wavenumber noise that cannot be explained without consideration of the above mechanisms are:

1) The inability of a perfectly valid linear model for the response of the TBL (Bark, 1975) to predict the measured (Morrison, et al., 1971) low wavenumber velocity fluctuation response to a burst.

2) The decrease in narrowband convention velocities found by Blake (1970) at small separation distances especially for frequencies below the spectral peak value.

3) The strong phase modulations among interacting waves of nearly equal wavenumbers measured explicitly by Miksad, et al. (1982) and shown inferentially by Blackwelder and Kaplan (1976).

4) The relatively low ($c \simeq 0.4U$) convection velocities of convected wall pressure fluctuation features measured by Emmerling, et al. (1973).

5) The full scale observation that the flow noise approximately doubles every 3 meters in the nose region of the vehicle.

We show that the interacting fluctuations are of spacial scale 2δ and lie at small angles ($\theta \leq 10^{\circ}$) to the wall. Therefore, we develops from first principles, design criteria for outer decouplers that defeat the low wavenumber flow noise in two ways:

(1) By responding to pressure fluctuations in a scale-selective fashion, transmitting with adequate fidelity the acoustic waves of interest but rejecting the fluctuation "carrier" components of scale 2δ.

(2) By rejecting the noise component that arrives at the decoupler at grazing incidence angles.

The resultant design constraints are manifold but achievable. Important desired properties are: a bulk density near to that of water, a longitudinal wave speed slightly above that of water and a bulk modulus to

shear modulus ratio above about 225. While isotropic materials cannot meet these criteria, anisotropic materials are available and viable. We further examine and specify support structure constraints.

Based on the foregoing we suggest an effort to:

1) Quantitatively and iteratively (with the materials fabricators) specify the optimum achievable material properties.

2) Assist and monitor the materials design/development process.

3) Evaluate and define materials attachment concepts and discontinuity effects.

4) Assist in field (KAMLOOPS) test planning and interpretation.

5) Assist in the analysis and interpretation of flow noise measurements.

2.0 THE TURBULENT BOUNDARY LAYER (TBL) FORCING FUNCTION

2.1 BACKGROUND

The wavenumber-frequency spectrum of wall pressure fluctuations is divided traditionally into three components deemed statistically independent: the convective component [characterized by $k \gtrsim (\omega/U)$], the low wavenumber component $[(\omega/c_a) \lesssim k \lesssim (\omega/U)]$ and the acoustic component $[k \lesssim (\omega/c_a)]$. The low wavenumber and acoustic components provide the significant noise sources for the large scale arrays considered in the ACSAS program. Unfortunately, only a modest body of relevant experimental information and a limited mechanistic understanding of the generation processes are available for those two components. The best available data (e.g., Jameson, 1975, Martin and Leehey, 1977) exhibit unexplained differences of about 10 dB between scaled low wavenumber spectral levels as a function of dimensionless frequency. In addition, the data are restricted to a range of wavenumbers, $0.2 \lesssim k\delta^* \lesssim 0.8$ that are over an order of magnitude higher than those of interest in practical applications where, for example, with $\omega = 100$ Hz, $k \simeq 4 \times 10^{-3}$ cm^{-1}, $U = 10^3$ cm/s, $L = 3 \times 10^3$ cm, $\delta^*(L) \simeq 2.9$ cm, one is concerned about $k\delta^*(L) \simeq 1.2 \times 10^{-2}$. Extrapolations remain quite uncertain because the data (Martin and Leehey, 1977) indicate

$$P(k,0,\omega)/(q^2\delta^{*3}/U) \propto (\omega\delta^*/U)^{-10/3} (k\delta^*)^0$$

while theory (Phillips, 1956) suggests

$$P(\underline{k},\delta) = 0(k^2)$$

in the incompressive limit. Finally, little guidance is provided for the evolution of outer decoupler concepts whose potential effectiveness against low wavenumber fluctuations is clearly contingent upon the fluctuation generation process.

The ORI effort has sought to address some of the aforenoted uncertainties about data extrapolations and desirable features of outer decoupler designs by constructing a rudimentary mechanistic view of boundary layer turbulence dynamics and its cause-effect relationships with the three components of the wavenumber-frequency spectra of wall pressure fluctuations. This viewpoint also provides a framework for rationalizing the scaling laws to be extracted from analysis of the experimental data generated under the ACSAS program and for identifying complementary approaches to the determination of the spectral components in question.

The particular mechanistic view of turbulence dynamics -- and its manifestations in the wall pressure fluctuations spectra -- depends on several supporting sets of considerations, namely: 1) the description of the coherent large scale structures/events revealed by recent fluid dynamic experiments employing conditional data sampling techniques in terms of cyclically self-reproducing, non-linear processes involving packets of finite-amplitude Tollmien-Schlichting waves intrinsically subject to large phase modulations; 2) the assessment of the significant, but incomplete, role of these non-linear wave processes in reproducing the salient aspects of available data for wall pressure fluctuation spectra, and the consequent evidence -- from both data and theory -- that a significant role is played by the continuous spectrum of modes of the turbulent boundary layer; 3) the determination of specific properties of the continuous spectrum -- largely ignored in previous studies of turbulent boundary layer dynamics -- that bear on the salient aspects of the wall pressure fluctuation data; 4) the indication that non-linear interactions between discrete spectrum (Tollmien-Schlichting) modes and continuous spectrum modes provide a plausible mechanism for the marked, experimentally observed, jitter of the coherent motions mentioned at 1 above and -- in line with recent findings about jet noise by Ffowcs-Williams and Kempton (1978) -- for the concurrent generation and characterization of the broadband low wavenumber as well as acoustic

components of the pressure fluctuation spectra. The four sets of considerations are set forth below in sequential paragraphs followed by a summary of the mechanistic view and its multifaceted implications for data acquisition, analysis and scaling as well as for outer decoupler design guidelines.

The emphasis on nonlinear aspects of the problem - explicitly indicated by the above list of considerations - stems directly from our interest in the low wavenumber and acoustic components of the wall pressure fluctuation spectra and from the straightforward observation that all linear modes of the turbulent boundary layer -- whether belonging to the discrete or to the continuous spectrum -- are characterized by phase velocity c smaller than, or at best equal to, the free stream velocity U. Thus, linear modes are characterized by wavenumbers $k \gtrsim (\omega/U)$ which can only contribute to the convective component of the spectrum. The low wavenumber and acoustic components (say k_3) must arise from nonlinear interactions among two or more linear modes (say k_1 and k_2) such that

$$\frac{k_3}{\omega_3} = \frac{k_1 - k_2}{\omega_1 - \omega_2} \lesssim \begin{cases} U^{-1} & \text{(Low wavenumber)} \\ c_a^{-1} & \text{(Acoustic)} \end{cases}$$

The requirement can be met, for example, with $k_1 \simeq k_2$ and $\omega_2 << \omega_1$. Accordingly, our inquiries are largely keyed to the following issues: 1) Do the discrete and continuous spectra of turbulent boundary layers include couples of modes that satisfy the noted requirement? 2) Does the mechanism of turbulence sustenance suggested by recent conditionally sampled measurements include the excitation of such couples of modes? 3) Do the available data for wall pressure fluctuation spectra -- especially their unresolved, puzzling aspects -- provide evidence that the considered couples of modes are indeed excited? These are the main issues discussed in the following paragraphs, although the discussion will at times depart from them to address additional aspects of the problem.

2.2 WAVE MECHANICS OF TURBULENCE GENERATION AND SUSTENANCE

Many of the considerations in this section were presented in an earlier ACSAS report (Vaglio-Laurin, Hoglund and Collier, 1982). They are repeated here to provide the reader with a single integrated exposition of our

views about boundary layer turbulence dynamics and its relationships to the three components of wall pressure fluctuation spectra.

According to the evidence submitted in the previous report a self-reproducing, deterministic cycle of wave-like processes determines the dynamics of the intermediate and low frequency modes in turbulent boundary layers. The cycle involves: a near-wall Reynolds stress burst that has limited spatial and temporal extent → a packet of finite-amplitude, oblique, Tollmien-Schlichting waves (representing part of the boundary layer response to the burst) that evolve on time/space scales much larger than those of the burst → oblique-wave-induced wall streaks and near-wall inflections of the instantaneous velocity profile that are subject to secondary Kelvin-Helmholtz instability → ejection of low momentum fluid from the wall and, thus, a Reynolds stress burst that restarts the cycle.

The nature of the cycle is largely determined by the following specific features of the finite amplitude oblique waves: 1) the profiles of the streamwise fluctuation velocity associated with an individual wave exhibit inflection points which, when viewed in wave-fixed coordinates, describe a locus that propagates downstream and away from the wall over a wavelength; 2) the profiles of streamwise velocity fluctuations associated with a pair of oblique waves are spanwise periodic and, therefore, characterized by inflection points only in a neighborhood of the "peaks," where the two waves reinforce each other; 3) oblique wave pairs interact nonlinearly with quasi two-dimensional (low k_z) waves of equal streamwise wavenumber (k_x) to yield locally inflectional distortions of the streamwise mean flow, also confined to a neighborhood of the "peaks"; 4) the superposed contributions of the streamwise velocity fluctuations and mean-flow distortion noted in 2) and 3) yield localized, hairpin-shaped, time-evolving inflections of the instantaneous velocity profiles which are ultimately subject to a secondary Kelvin-Helmholtz instability; 5) concurrent with the formation of inflectional profiles, oblique-wave pairs subject the near-wall region to a spanwise component of velocity (periodic in time as well as in the spanwise space coordinate) which results in the formation of wall streaks and the periodic ejection of low-momentum fluid from the wall (Blackwelder and Eckelmann 1979, Hatziavramidis and Hanratty 1979).

The oblique waves in question are those associated with the peaks of the velocity fluctuation spectra measured by Morrison et al., (1971) and with the largely coincident peaks of the spectra predicted by Bark's (1975) calculations of the response to a burst including only the contribution of the Tollmien-Schlichting modes (Figures 2.1 and 2.2). The experiments of Blackwelder and Kaplan (1976) clearly establish that the dynamics of these waves is controlled by deterministic processes and is characterized by an amplitude-dependent dispersion relation which renders them susceptible to large amplitude modulations. Specifically, Blackwelder and Kaplan used the variable-interval-time-averaging (VITA) technique to detect bursts in a flat-plate turbulent boundary layer. The VITA detection criterion depends upon a threshold value of the squared streamwise fluctuation velocity. As the threshold value is increased only the more intense coherent events are detected and higher conditionally-averaged signatures are obtained. However, if the process responsible for the signatures is truly deterministic -- as implied by our views -- the conditional averages at different threshold levels must scale with the threshold value. This requirement is supported remarkably well by the data obtained with threshold-value variations of as much as a factor of three, provided the detection and the sampling take place at the same location (Figure 2.3a).

In spite of their amplitude-independent structure, the coherent velocity signatures possess a random convection velocity as revealed by Blackwelder and Kaplan's attempt to follow the downstream evolution of the signatures. For that purpose the conditionally averaged Reynolds stress was measured at the detection station (top trace in Figure 2.3b) and, after an appropriate time delay, also at a station displaced downstream by $\Delta x = (\delta/4)$. The middle trace in Figure 2.3b displays the results of the averaged stress measurements at the latter station obtained with a fixed time delay corresponding to the average convection velocity. The original strong Reynolds stress has disappeared almost completely. This result was quite surprising because, if the bursting phenomenon is so important in the turbulence production process, then the Reynolds stress associated with this phenomenon should not die out so quickly downstream. After exploring several different explanations, Blackwelder and Kaplan recognized that the result was spurious in that random minor variations in the convection velocity combined

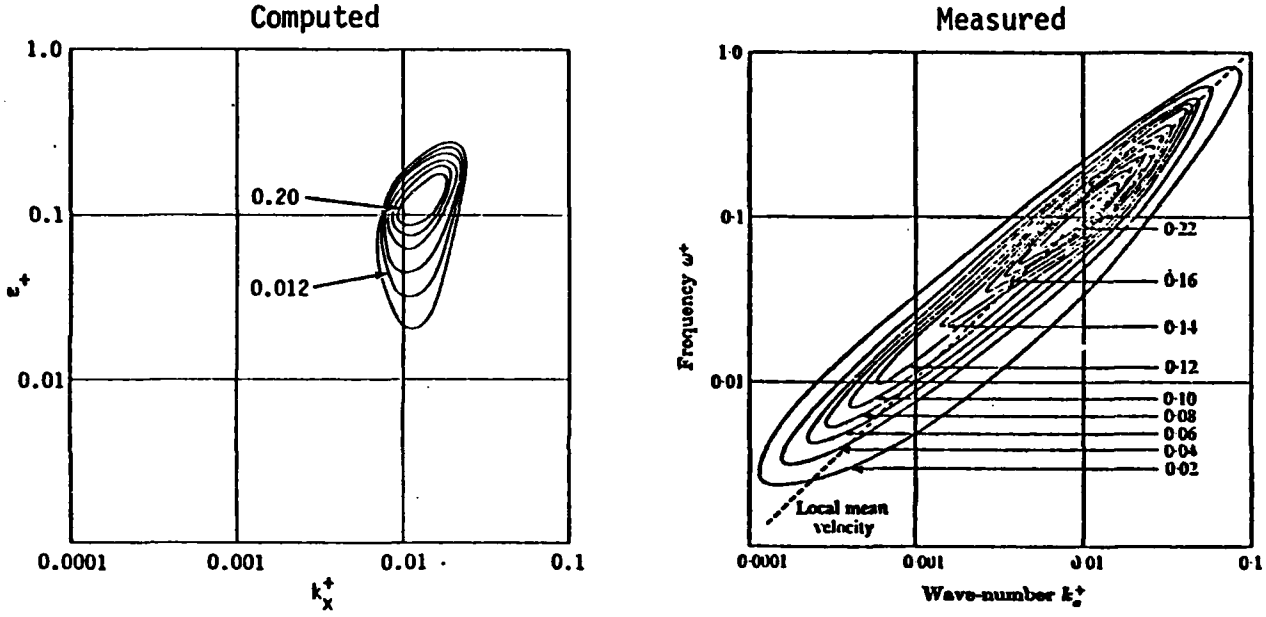

FIGURE 2.1 FREQUENCY - WAVENUMBER SPECTRUM OF VELOCITY FLUCTUATION RESPONSE TO A BURST COMPUTED BY BARK (1975) AND ITS COMPARISON WITH THE MEASUREMENTS OF MORRISON et al., (1971)

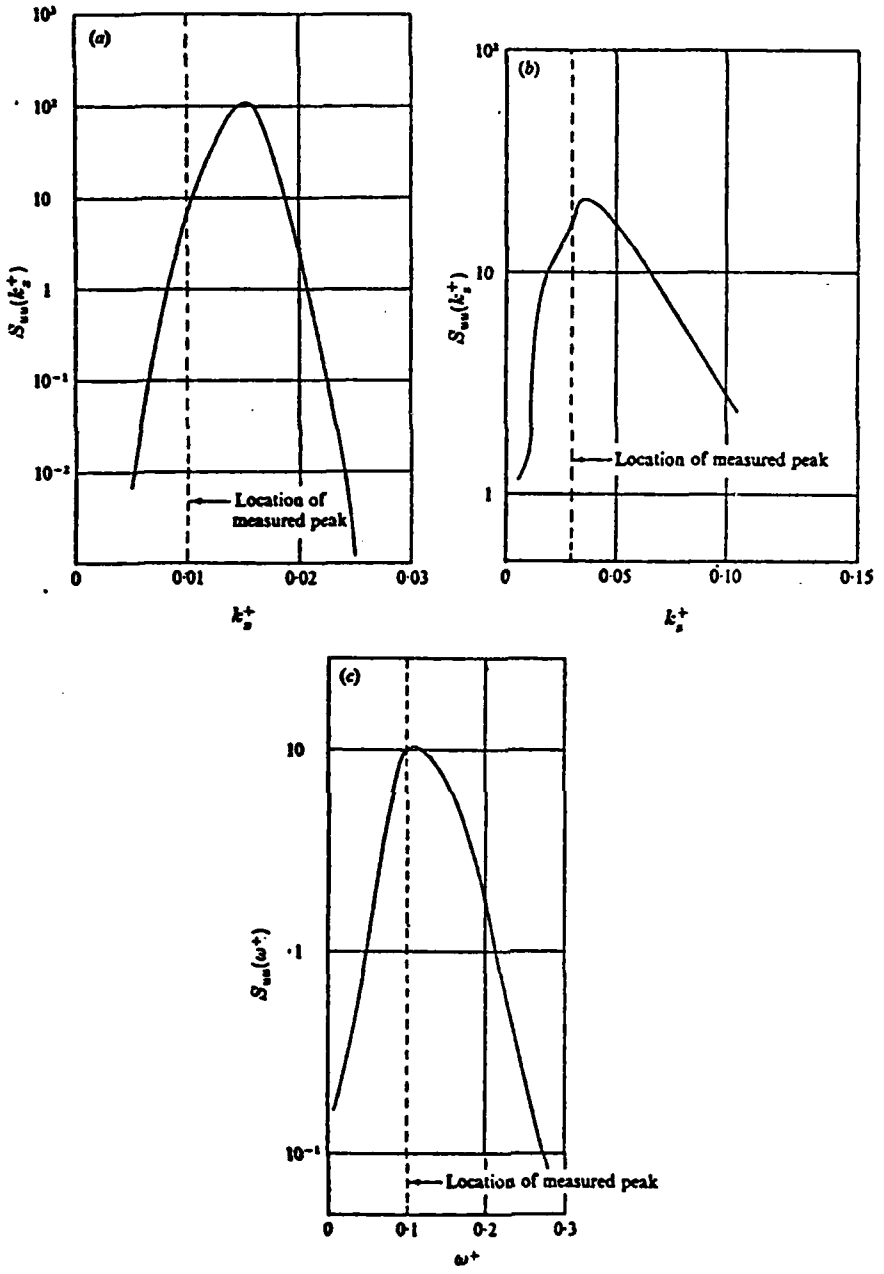

FIGURE 2.2 COMPUTED VELOCITY FLUCTUATION SPECTRA AT $y^+ = 15$ (FROM BARK, 1975), ALONG WITH MEASURED PEAKS (FROM MORRISON et al., 1971).

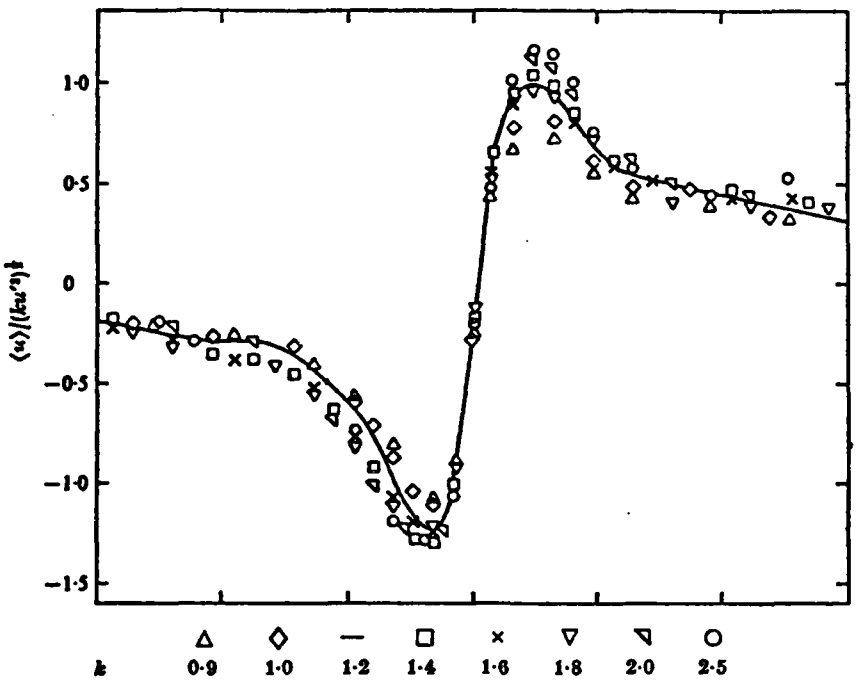

FIGURE 2.3a CONDITIONAL AVERAGE OF STREAMWISE VELOCITY COMPONENT AT VARIOUS THRESHOLD LEVELS (FROM BLACKWELDER AND KAPLAN, 1976)

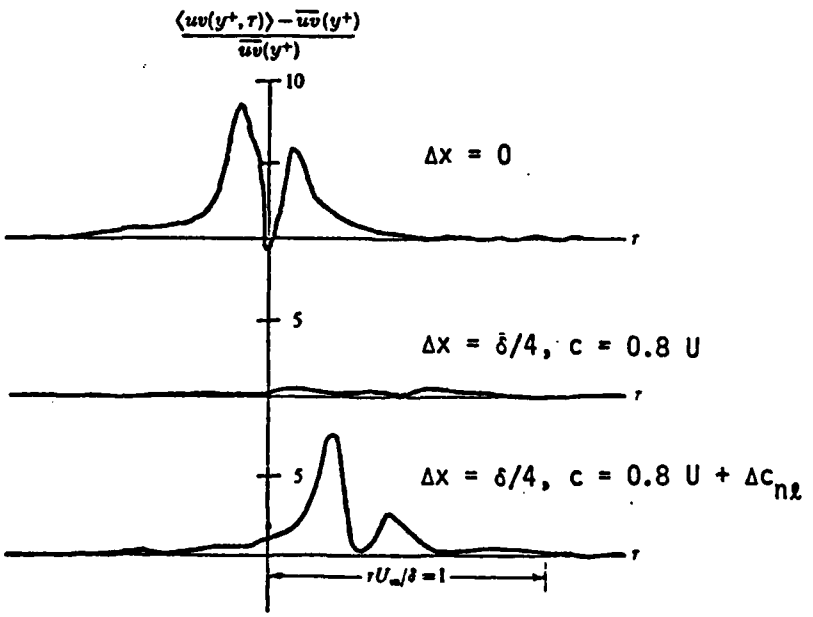

FIGURE 2.3b CONDITIONAL AVERAGES OF THE REYNOLDS SHEAR STRESS (FROM BLACKWELDER AND KAPLAN, 1976)

with the short duration peaky nature of the signature to invalidate its conditional average at fixed time delay. The difficulty was overcome by again applying the detection criterion at the downstream station. Then, if the time difference between detection at the upstream and downstream positions was within the limits established by the maximum and minimum values of the convection velocity, the Reynolds shear stress was conditionally averaged with respect to the downstream detection time. By this process Blackwelder and Kaplan recovered the results displayed in Figure 2.3b as the lowermost trace with the time shift taken as the average delay of observations in the ensemble average. As can be seen, most of the Reynolds stress is still evident, although some decay is apparent. Unfortunately Blackwelder and Kaplan report neither the statistics of the minor random convection velocity variations nor the correlation between those variations and the much larger ones in the signature amplitude. Nevertheless, an amplitude-dependent dispersion relation is strongly indicated since the shape and spectral content of the signature are insensitive to amplitude variations (Figure 2.3a). The analytical considerations presented in Appendix A permit calculation of this amplitude dependence from first principles.

The amplitude-dependent dispersion relation (A - 27) is of the form

$$\omega = \omega_o(k, |A|^2) \tag{1}$$

In the presence of an amplitude modulation $|A|_m$ -- such as accrues to sequential realizations of the wave motions representing the coherent TBL response to a burst according to the conditionally averaged measurements of Blackwelder and Kaplan reported in Figure 2.3a -- the dispersion relation (1) can be expanded in the form

$$\omega = \omega_o(k, |A|_o^2) + \left(\frac{\partial \omega}{\partial |A|^2}\right)_o |A|_m^2 + \ldots \tag{2}$$

where $(\partial\omega/\partial|A|^2)_o$ denotes the derivative computed at $|A| = |A|_o$, the amplitude averaged over the ensemble of possible realizations. The frequency deviation exhibited in (2), viz

$$\delta\omega = (\partial\omega/\partial|A|^2)_o \, |A|_m^2 \tag{3}$$

is equivalent to a phase modulation. Indeed, if one writes the stream function associated with the dominant wave motion in the form

$$\psi(x,y,t) = |A(x,t)|\zeta(y) \cos [k_o x - \omega_o t + p(x,t)] \tag{4}$$

where $|A(x,t)|_m = |A(x,t)| - |A(x)|_o$ and $p(x,t)$ are slowly varying amplitude and phase modulations, one can readily determine the deviation of the instantaneous frequency ω from the carrier frequency ω_o, viz

$$\delta\omega = \omega - \omega_o = -(\partial p/\partial t) \tag{5}$$

A comparison of (3) and (5) then yields

$$(\partial p/\partial t) = -(\partial\omega/\partial|A|^2)_o \; |A|_m^2 \tag{6}$$

which shows that, because of the amplitude-dependent dispersion relation, the Tollmien-Schlichting waves partaking in the TBL response to a burst are subject to amplitude-modulation-induced phase modulations, and vice versa.

If the amplitude modulation were known -- e.g., from an examination of the time series for variable threshold measurements such as those by Blackwelder and Kaplan compiled in Figure 2.3a -- and the phase modulations were determined accordingly -- by integration of (6) -- the spectrum of the modulated wave motion could easily be calculated. Indeed, it is well known (Kim et al., 1980) that in the model situation where $|A(x)|_o$ is independent of x and

$$|A(x,t)|_m = \alpha \sin(\chi x - \nu t + \Theta)|A|_o \tag{7-a}$$

$$p(x,t) = \beta \sin(\chi x - \nu t) \tag{7-b}$$

the spectrum of the wave motion (4) is

$$\psi(x,y,t) = \sum_{m=-\infty}^{\infty} A_n \, \zeta(y) \cos(k_n x - \omega_n t + \phi_n) \tag{8}$$

with

$$A_n^2 = \left(1 + \frac{\alpha n}{\beta}\sin\Theta\right)^2 J_n^2(\beta) + (\alpha\cos\Theta)^2 (dJ_n/d\beta)^2 \tag{9-a}$$

$$k_n = k_o + n\chi \tag{9-b}$$

$$\omega_n = \omega_o + n\nu \tag{9-c}$$

$$\phi_n = \tan^{-1}\left[\frac{\alpha\cos}{1 + (\alpha n/\beta)\sin\Theta} \frac{dJ_n/d\beta}{J_n(\beta)}\right] \tag{9-d}$$

where J_n denotes the Bessel function of order n and argument β. Unfortunately, this simple model proves inadequate to reconcile the wide differences exhibited in Figure 2.1 between the velocity fluctuation spectra calculated by Bark (1975) and those measured by Morrison et al., (1971). The measured spectral ridge coincides with a line $(\omega/k) \simeq$ constant (say $c_o < U$) for

$k \gtrsim k_0$ and $\omega \gtrsim \omega_0$, but progressively shifts toward $c_0 < (\omega/k) \rightarrow U$ as k and ω decrease below the peak values k_0, ω_0. The proportionality $(\chi/k_0) \simeq (\nu/\omega_0)$ implied by the behavior of the upper sidebands is then violated by the lower sidebands.

The behavior of the measured spectral ridge for $k \gtrsim k_0$ and $\omega \gtrsim \omega_0$ differs significantly from Blake's (1970) finding that narrow band convection velocities decrease by a factor 1.4 as the frequency increases by a factor 5 over the spectral peak value (Figure 2.4). The Morrison data (Figure 2.1) suggests that at least the high frequency-high wavenumber portion of the spectrum is dominated by a modulation due to nonlinear interactions among the waves of nearly equal wavenumber associated with the narrow spectral peak calculated by Bark (Figure 2.2). Since these waves are nearly resonant (Figure 2.5), their coupling is quite efficient. A strong phase modulation ensues according to the theoretical considerations of Appendix B (adapted from the work of Kim et al., 1980) as well as according to some recent measurements of velocity fluctuations obtained by Miksad et al., (1982)* in the transitional wake of a thin two-dimentional airfoil exposed to a $U = 8.4$ m s^{-1} air stream. A brief review of these measurements vividly illustrates the rapid build-up of the modulation within wave convection distances $\Delta x \simeq 3\lambda$ which coincide with the damping distances of the dominant waves in the TBL indicated by attendant narrowband correlations of wall pressure fluctuations at and above the spectral peak frequency.

---

* Dr. Miksad's permission to quote his yet unpublished results is acknowledged gratefully.

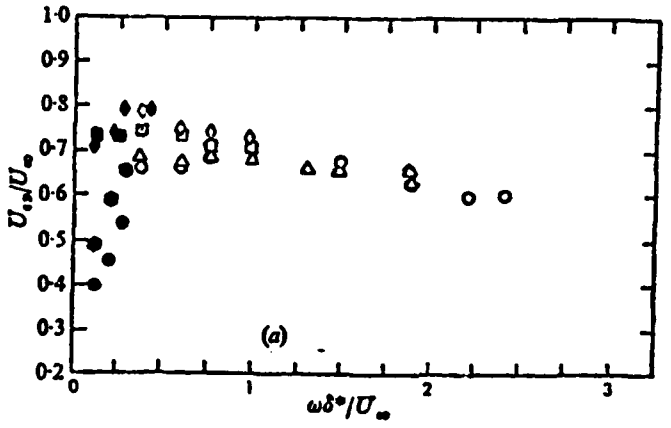

FIGURE 2.4 PHASE CONVECTION VELOCITIES INDICATED BY NARROWBAND CORRELATIONS OF WALL PRESSURE FLUCTUATIONS (FROM BLAKE, 1970)

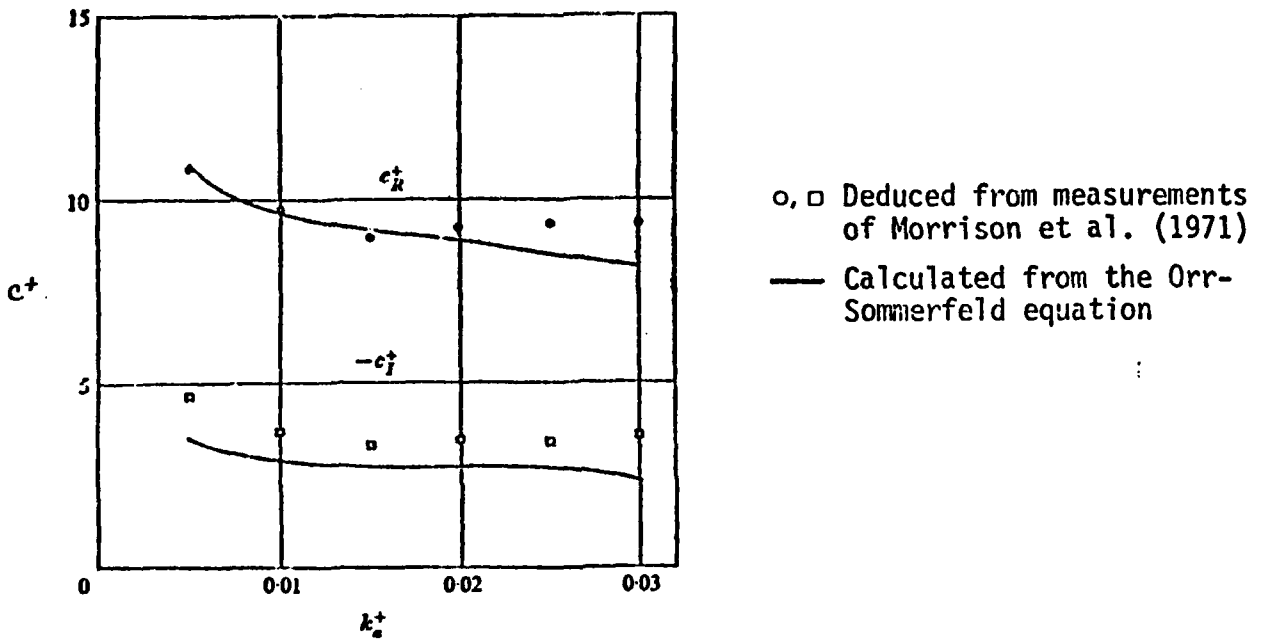

FIGURE 2.5 CALCULATED AND OBSERVED REAL AND IMAGINARY PARTS OF THE STREAMWISE PHASE VELOCITY OF THE TOLLMIEN-SCHLICHTING WAVES EXCITED BY A BURST IN A TBL (FROM BARK, 1975)

The initial width of the wake investigated by Miksad et al., is $b \simeq 10^{-3}$ m and the initial velocity defect $(U - U_c) \simeq 1.6$ m s^{-1}. Acoustic sources are used to excite simultaneously two unstable frequencies $f_o = 550$ Hz and $f_1 = 582$ Hz with wavelength $\lambda \simeq .015$ m. The two frequencies grow linearly without evidence of significant interactions up to a distance $x = .01$ m downstream of the airfoil trailing edge. The power spectrum of the velocity fluctuations at this station -- displayed on the top left of Figure 2.6 -- exhibits dominant sharp peaks at the two forced frequencies accompanied by an emerging fluctuation at the difference frequency $f_\nu = f_o - f_1$. Nonlinear wave-wave interactions rapidly evolve at stations $x > .01$ m. The result three wavelengths downstream ($\Delta x \simeq .05$ m, $x \simeq .06$ m) is that the power spectral density increases about one hundred-fold over a broad range of frequencies (see Figure 2.6, $x = 6$ cm). The nonlinear evolution of the spectrum continues further downstream; however, the consequences over relatively large distances (e.g., between $x = 6$ cm and $x = 30$ cm in Figure 2.6) are quite moderate compared to those observed during the initial interaction. Significantly the filling of the spectrum (at $x \lesssim 6$ cm) as well as its subsequent evolution can be associated with amplitude and phase modulations of the dominant frequency f_o. Miksad et al. prove this point by applying the digital complex demodulation procedures of Khadra (1981) to the velocity fluctuations waveforms displayed on the left of Figure 2.7. By those procedures the amplitude (a_m) and the phase (p_m) modulations attendant to the representation

$$u'(\underline{x},t) = a_o[1 + a_m(\underline{x},t)] \cos[k_o x - 2\pi f_o t + p_m(\underline{x},t)]$$

of the waveforms are obtained. The results displayed at the center and right of Figure 2.7, show that the amplitude modulation is relatively modest while the phase modulation becomes quite large (the phase modulation scale in Figure 2.7 is ± 6 rad). In line with the expectations set forth in Appendix B the strong phase modulation process is largely accomplished within the first three

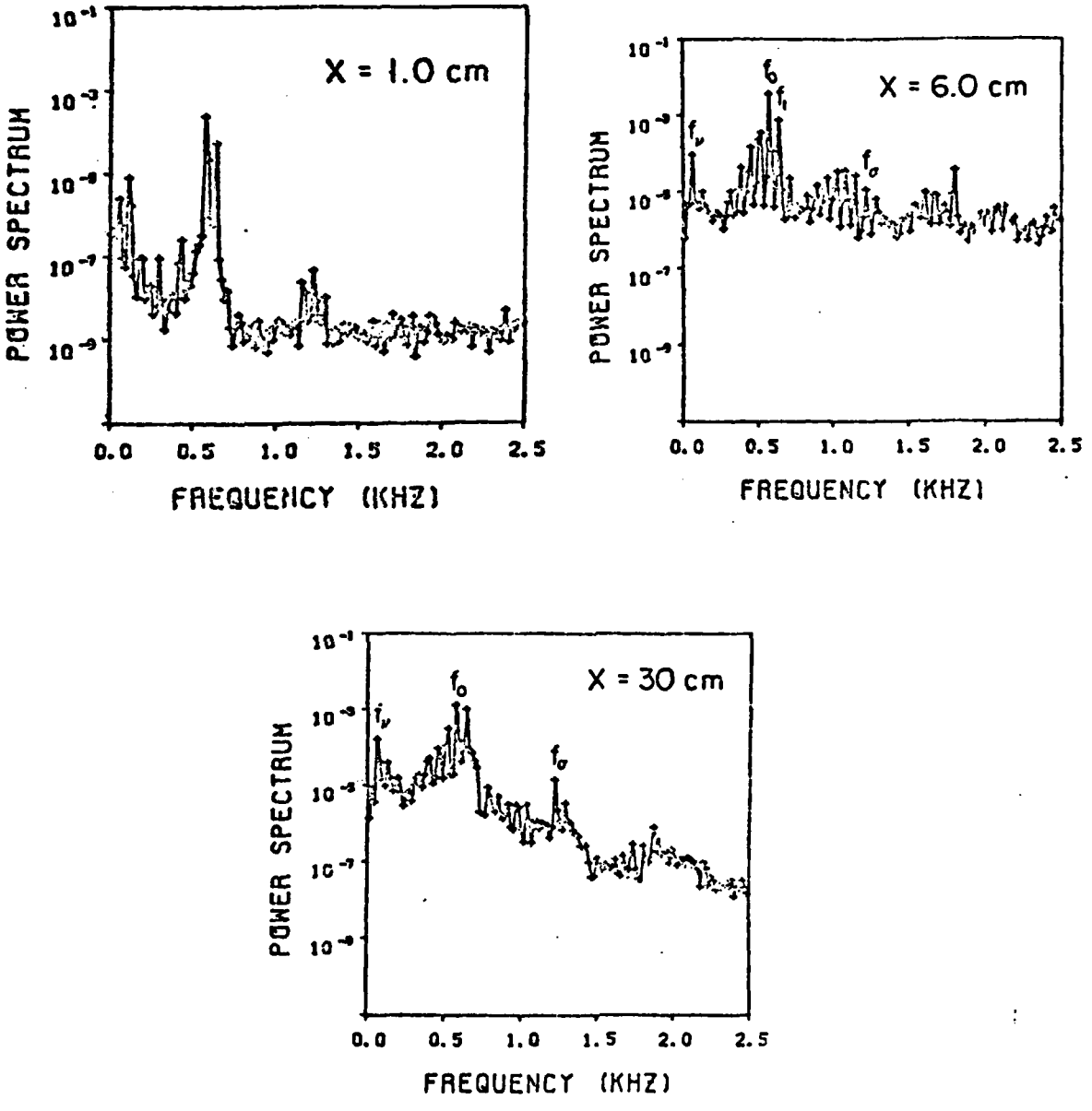

FIGURE 2.6 SUBSEQUENT DOWNSTREAM POWER SPECTRA OF LONGITUDINAL VELOCITY FLUCTUATIONS (FROM MIKSAD et al., 1982)

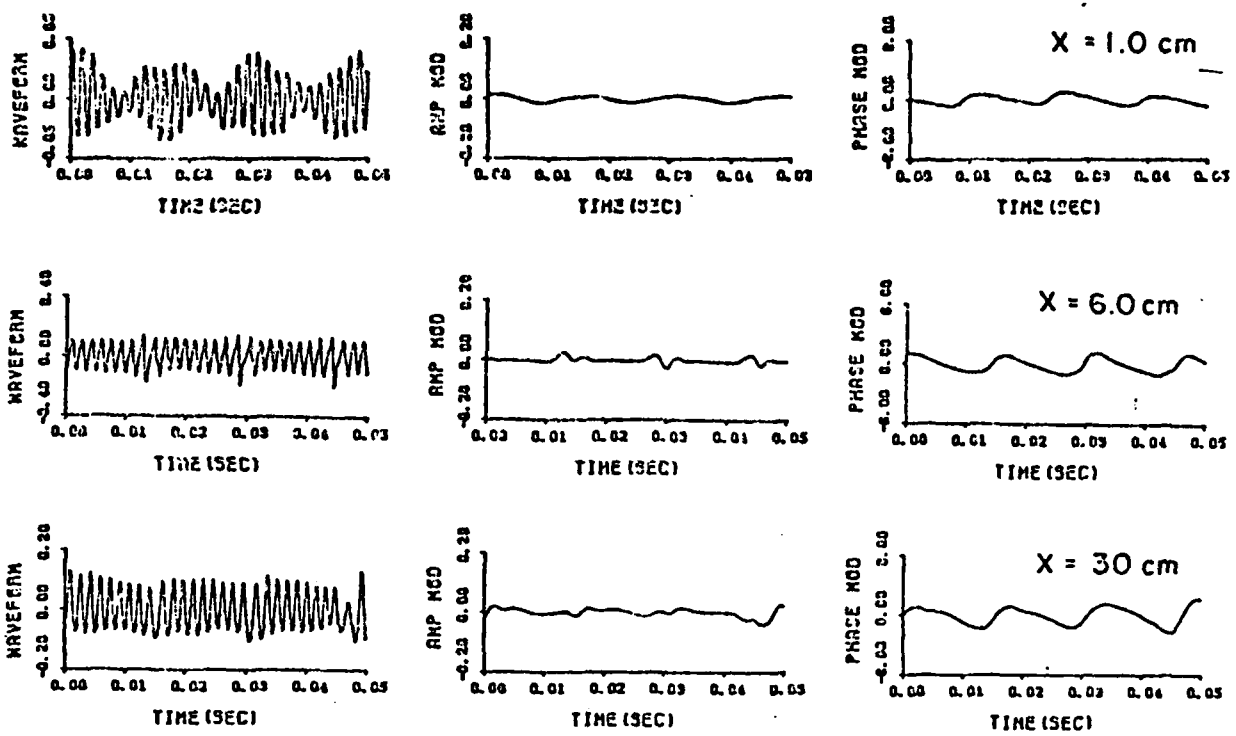

FIGURE 2,7 SUBSEQUENT WAVE FORMS, AMPLITUDE MODULATIONS AND PHASE MODULATIONS FOR THE POWER SPECTRA OF FIUGRE 2,6 (FROM MIKSAD et al., 1982)

wavelengths and remains close to being a simple sinusoid at the difference frequency f_ν throughout the process.

Inspection of the results of Appendix B for the amplitude and phase modulation indices [see (B-7a) and (B-7b)] readily shows that even a modulation driven by the nonlinear interaction of nearly resonant waves does not explain several significant aspects of the data, namely: 1) the distinct convection velocities exhibited by the ridge of the measured convective component of the velocity fluctuations spectrum at low and high frequencies (Figure 2.1); 2) the presence of modes having high subsonic and supersonic convection velocities as accrue, respectively, to the low wavenumber and acoustic components of the spectra; 3) the large amplitude variations exhibited by the ensemble of coherent motion realizations observed by Blackwelder and Kaplan (Figure 2.3a); 4) the large, experimentally observed, seemingly random space/time jitter of sequential realizations of the coherent motions that is required to yield the experimentally observed smooth growth of the mean TBL flow. Clearly we must question the assumption implicit to wavemechanical models of turbulence that Tollmien-Schilichting modes and/or their nonlinear interactions dominate the problem. Other modes must be present and they must be associated with the continuous spectrum of the TBL, a component which has generally been ignored except for Gustavsson's (1979) study of the initial value problem for laminar boundary layer flows in the linear limit.*

A little reflection readily indicates the significance of the omission. Recent studies of laminar boundary layers keyed to the determinaton of the higher eigenvalues of the Orr-Sommerfeld equation (Mack 1976, Corner et al., 1976) show that for any combination of wavenumber and Reynolds number there is only a finite, and small, number of discrete Tollmien-Schlichting eigenvalues. But a finite set of eigenfunctions cannot be a complete set. The correct expansion of an arbitrary initial disturbance -- such as that imposed by a burst in a TBL -- must include the continuous spectrum. Specifically, the

---

* Gustavsson points out the requirement that the continuous spectrum be included but does not exhibit its effect on flow evolution even in the linear limit.

stream function of a strictly two-dimensional flow even in the linear approximation must be described by

$$\psi = \int_{-\infty}^{\infty} \{ \sum_n A_n(k)\ \phi_n\ (y,k)\ \exp\ [ik\ (x - c_n t)] + \int_0^U B(k,c)\ \phi\ (y,k,c)\ \exp\ [ik(x - ct)]\ dc \}\ dk \qquad (10)$$

where the summation term and the subsequent integral term, respectively, reflect the contributions of the discrete (Tollmien-Schlichting) spectrum and the continuous spectrum. Admittedly the higher modes of the discrete spectrum are highly damped and, therefore, can be neglected compared to the first mode as in Bark's calculations. However, the continuous spectrum -- as shown in Section 2.4 -- includes modes subject to less damping than the first mode Tollmien-Schlichting waves and, therefore, cannot be neglected. For the purposes of this report we must then ask whether the inclusion of the continuous spectrum can rationalize the aforelisted unsolved aspects of the data. The evidence to that effect is set forth in the following paragraphs.

2.3 SOME ASPECTS OF WALL PRESSURE FLUCTUATIONS SPECTRA

We begin by reviewing wall pressure fluctuation frequency spectra for turbulent boundary layers on smooth and rough flat plates (e.g., Blake, 1970; Willmarth, 1975). These measurements indicate that three frequency (ω) ranges may be recognized in the spectra $\phi(\omega)$ scaled with respect to outer variables U (freestream velocity) and δ^* (boundary-layer displacement thickness): a high-frequency range $(\omega\delta^*/U) \gtrsim 2$; an intermediate-frequency range $0.3 \lesssim (\omega\delta^*/U) \lesssim 2$; and a low-frequency range $(\omega\delta^*/U) \lesssim 0.3$.

<u>At high frequencies</u> the frequency spectra correlate in the functional form dictated by inner variables; with the notation q for the dynamic pressure, u_τ for the shear velocity, c_f for the skin friction coefficient, k_g for the mean roughness height, and ν for the kinematic viscosity, this form is:

$$[\phi(\omega)/q^2]\ [\nu/u_\tau{}^2]^{-1}\ \text{vs}\ \omega(\nu/u_\tau{}^2)$$

for smooth walls and

$$[\phi(\omega)/q^2]\ [k_g c_f{}^2/u_\tau]^{-1}\ \text{vs}\ \omega(k_g/u_\tau)$$

for rough walls. The narrowband convection velocities are found to be frequency-independent but roughness-dependent (approximately 0.6 U for smooth walls and 0.45 U for rough walls).

At intermediate frequencies the spectra over smooth as well as rough walls correlate in the functional form dictated by the outer variables, viz

$$[\phi(\omega)/q^2]\ [\delta^* c_f^2/U]^{-1} \quad \text{vs} \quad \omega(\delta^*/U)$$

The narrowband convection velocities are frequency -- as well as roughness -- dependent; for example, they vary from 0.6 U to 0.8 U as the frequency decreases for the smooth-wall case.

At low frequencies the scaling remains uncertain. Reference to the outer variables fails to correlate the spectra over rough walls. The narrowband convection velocities decrease sharply with frequency when measured at small separations, but show considerably less frequency dependence when mesured at large separations; the levels measured at small separation fall distinctly below those associated with the high and intermediate frequencies (Figure 2.4).

The behavior of the spectra at high and intermediate frequencies is consistent with a wave-like nature of the attendant sources. In fact Landahl (1967) and Bark (1975) have demonstrated that the intermediate-frequency fluctuations constitute the large-scale response of the boundary layer to the localized stress pulses caused by the periodic bursting process evidenced in numerous turbulent boundary-layer studies (e.g., Kim et al., 1971). The analytically determined response reproduces many of the experimentally observed features in the smooth-wall case. For wavenumbers above the spectral peak, the phase speed decreases with an increase in wavenumber from a value of 0.8 U_∞ at low wavenumbers to a value of 0.6 U_∞ at high wavenumbers (Figure 2.4 and 2.5). The calculated decay rate provides an e-fold amplitude decrease within a travel distance of 1.5 wavelengths in line with that indicated by the measured longitudinal cross-spectral densities of wall pressures. The predicted U-fluctuation spectra in the wall region (Bark 1975) peak at frequencies and wavenumbers in reasonable agreement with the measured data of Morrison et al., (1971) (Figure 2.2). However, the computed peaks are considerably narrower than the measured ones for the ($\omega_1 k_x$) spectra (compare

the regions $k_x^+ \gtrsim 10^{-2}$ in Figure 2.1) while they are comparable to those observed for the $(\omega_1 k_z)$ spectra. The latter comparison supports the interpretation set forth in Section 2.2 and in Appendix B that the relatively rapid decay of the spectral ridge computed in the linear limit is due to a phase modulation driven by nonlinear interaction among the dominant waves.

As noted in Section 2.2 the low frequency portion of the measured spectra ($\omega^+ < 10^{-1}$ in Figure 2.1) is not explained by either the Landhal-Bark linear viewpoint or the nonlinear modulational viewpoint. The low frequency, low wavenumber modes evidenced by the measurements cannot be linear Tollmien-Schlichting modes because these have all been included in Bark's calculations; the results displayed in Figure 2.1 indicate that the contribution of the low wavenumber Tollmien-Schlichting modes is rejected in the process of convolving the second derivative of the eigenfunctions -- which possesses distinct sensitivity to wavenumber -- with the shape of the forcing stress pulse to determine the response. The nonlinear modulational viewpoint does not reproduce the convection velocities associated with either the spectral ridge of Figure 2.1 or the narrowband correlation measurements of Figure 2.4. Significantly, the narrowband correlation measurement at low frequency indicate low convection velocities $c \simeq .4\ U$ distinctly below those at intermediate and high frequencies but comparable to those of the intense, convected, positive wall pressure features exhibited by Emmuerling et al.'s (1973) observations of instantaneous spatial patterns of wall pressure fluctuations (Figure 2.8). These features at first are roughly circular with streamwise extent of the order of $0.5\delta^*$ and then become larger in the cross-stream directions while they travel downstream. They retain their identity over downstream distances of the order of $9\delta^*$ and, thus, exhibit a ratio ($\simeq 18$) between decay distance and streamwise extent greatly exceeding that ($\simeq 6$) revealed by the narrowband correlations and the linear response calculations. As such, they can hardly be associated with Tollmien-Schlichting modes. We submit that they reflect continuous spectrum modes which -- as shown in the next paragraph -- possess convection velocity and damping distinctly lower than those of the Tollmien-Schlichting waves. We have argued in Section 2.2 that the continuous spectrum modes are part and parcel of the TBL response; the experimental evidence presented here proves

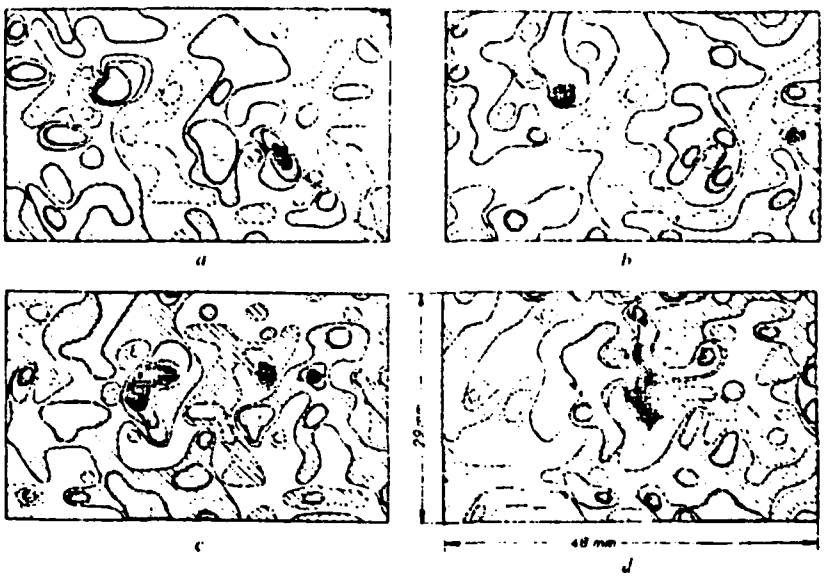

FIGURE 2.8 CONTOURS OF INSTANTANEOUS PRESSURE FLUCTUATIONS (EMMERLING, et al., 1973) SHOWING AN INTENSE LONG-LIVED POSITIVE CONTRIBUTION WITH INITIAL STREAMWISE EXTENT $\ell \simeq .5\ \delta^*$ AND CONVECTION VELOCITY $c \simeq .39\ U$.

that they provide a measurable contribution to the convection component of wall pressure fluctuation spectra.

2.4 SOME PROPERTIES OF THE TBL CONTINUOUS SPECTRUM

The available information about continuous spectra of boundary layers is limited to the sparse results recently presented by Grosch and Salwen (1978) and Salwen and Grosch (1981) for laminar Blasius flow. Fortunately some of the results can readily be extended to the TBL problem of interest here.

The continuous spectrum of the Orr-Sommerfeld equation for a two-dimensional spatially developing flow contains four branches. In terms of dimensionless variables scaled to the boundary layer displacement thickness δ^* and the boundary layer edge velocity U the first two branches of the continuous spectrum are characterized by the dispersion relation

$$k_{1,2} = \pm (\omega/\gamma) - iR[(1 \pm \gamma)/2 \pm (\omega/R)^2/\gamma^3] + O(\omega^3/R^2) \qquad (11)$$

where k denotes wavenumber, ω frequency, R Reynolds number and $\gamma = (1 + 4m^2/R^2)^{\frac{1}{2}}$ in terms of a parameter m that can vary between 0 and ∞.

Equation (11) can be greatly simplified in the limits $m \to 0$ and $m \to \infty$. With the phase velocity defined by

$$c_{1,2} = k^*_{1,2}\, \omega/|k_{1,2}|^2$$

(where * denotes complex conjugate) one obtains

$4(m/R)^2 \ll 1$

$$k_1 = \omega[1 - 2(m/R)^2] + iR[(\omega/R)^2 + (m/R)^2] \qquad (12\text{-a})$$

$$k_2 = -\omega[1 - 2(m/R)^2] - iR[1 + (\omega/R)^2 + (m/R)^2] \qquad (12\text{-b})$$

$$c_1 = 1 - [(\omega/R)^4 + (m/R)^4](\omega/R)^{-2} - i[(\omega/R)^2 + (m/R)^2](\omega/R)^{-1} \qquad (12\text{-c})$$

$$c_2 = -(\omega/R)^2 + i[1 + (\omega/R)^2 + (m/R)^2](\omega/R) \qquad (12\text{-d})$$

$4(m/R)^2 \gg 1$

$$k_1 = (\omega/2)(m/R)^{-1} + im \qquad (13\text{-a})$$

$$k_2 = -k_1 \qquad (13\text{-b})$$

$$c_1 = \tfrac{1}{2}(\omega/R)^2(m/R)^{-3} - i(\omega/R)(m/R)^{-1} \qquad (13\text{-c})$$

$$c_2 = -c_1 \qquad (13\text{-d})$$

Clearly the eigenfunctions on branch 1 represent downstream traveling waves while those on branch 2 represent upstream traveling waves. All of these waves decay strongly as they travel except for the subset of branch 1 characterized by $(m/R)^2 \lesssim R^{-1} << 1$, which possesses modest damping rate Im(k) and nearly unit phase speed Re(c).* Only this subset is of interest for our considerations because the eigenfunctions on branches 3 and 4 prove to be standing waves varying like exp(±mx).

As $y \to \infty$ the considered eigenfunctions exhibit the normalized, constant amplitude, oscillatory behavior

$$\psi(x,y,t) \approx \exp[i(kx + my - \omega t)] + B \exp[i(kx - my - \omega t)] + C \exp[-Re(k)y + i(kx - \omega t)] \qquad (14)$$

which is bounded, not exponentially decaying. However, wave packets that behave like $\exp(-k_o y)$ can be constructed by selection of appropriate (k, ω) spectra such as that which describes the linear response of the boundary layer to a localized vorticity disturbance periodic in time, viz.

$$\nabla^2\psi \propto \delta(x - x_o)\, \delta(y - y_o) \exp(-i k_o c_o t)$$

A little reflection on the results (12-a, d) and (14) is illuminating. Let's first consider the eigenfunctions on branch 1 characterized by $(m/R)^2 = f R^{-1}$ where f is a quantity of order unity, comparable to the frequency ω. The damping rate and the phase velocity for these eigenfunctions are Im(k) = f and $Re(c) = 1 - (f/\omega)^2$, respectively, according to (12-a) and (12-c). Since $Re(k) \simeq \omega$ per (12-a), we see that $Im(k)/Re(k) = (1 - c)^{\frac{1}{2}}$ and, for a fixed Re(k) and ω, the damping rate increases as the phase velocity decreases. But this is exactly the behavior displayed by Blake's narrowband correlation measurements (Figure 2.4) where the convection velocity increases markedly with the separation distance, especially for frequencies below that of the spectral peak, $\omega \lesssim .3$. Thus, we interpret the observed dependence of the convection velocity upon separation distance as evidence that significant continuous spectrum modes are excited in

---

* Representative values of the quantities appearing in (12-a,d) and (13-a,d) for situations of practical interest are: $\omega \approx O(1)$, $R \simeq O(10^4)$, $\delta^* \simeq O(.5cm)$ for wind tunnels experiments; $\omega \simeq O(1)$, $R \simeq O(10^5)$, $\delta^* \simeq O(.5cm)$ for water tests with quarter scale models.

the boundary layer. Further support for this view is gained by a reexamination of the velocity fluctuation spectra first displayed in Figure 2.1. Selected constant power density contours from Figure 2.1* are replotted in Figure 2.9 together with lines of constant convection velocity. The measurements clearly associate significant power with modes characterized by $.7 \lesssim (c/U) \lesssim 1$ and frequency smaller than twice the peak frequency (region 1 of Figure 2.9). Since the power densities in region 1 equal or exceed the square of the peak power density we can hardly attribute the modes in question to nonlinear interactions among Tollmien-Schlichting modes of near peak power. This is the same conclusion reached in Section 2.2 on the basis of convection velocity considerations, and just above on the basis of the separation distance dependence of narrowband convection velocity measurements.

Significantly the experimental data in Figure 2.9 associate measurable power with modes characterized by convection velocities $1 \lesssim (c/U) \lesssim 1.6$ (see region 2 in the figure). These modes, which belong to the low wavenumber component of the spectrum, cannot be linear modes because $(c/U) < 1$ for both the discrete (Tollmien-Schlichting) and the continuous spectra; hence, they must reflect the result of nonlinear interactions among components of those spectra. At present we cannot specifically identify the interactions in question because our results pertain to the strickly two-dimensional continuous spectrum, while in a TBL we anticipate that, due to the highly localized nature of the bursting process, highly oblique continuum modes are excited, much as we know to be the case for the discrete modes from Ba·k's calculations.**

---

* Figures 2.1 and 2.9 follow the practice by Morrison et al., (1971) of displaying the densities $P(k_x,\omega)$ related to the two-dimensional spectra $\phi(k_x,\omega)$ by $P(k_x,\omega) = k_x\omega\ \phi\ (k_x,\omega)\big|$. With logarithmic scales for k_x and ω, and a linear scale for $P(k_x,\omega)$, the energy in a particular frequency - wavenumber band is directly proportional to the volume under the surface displayed in the figure.

** The long lived, small scale positive wall pressure feature revealed by Emmerling's experiments (Figure 2.8) is clearly three-dimensional. Its analytic reconstruction must await the determination of the 3D continuum.

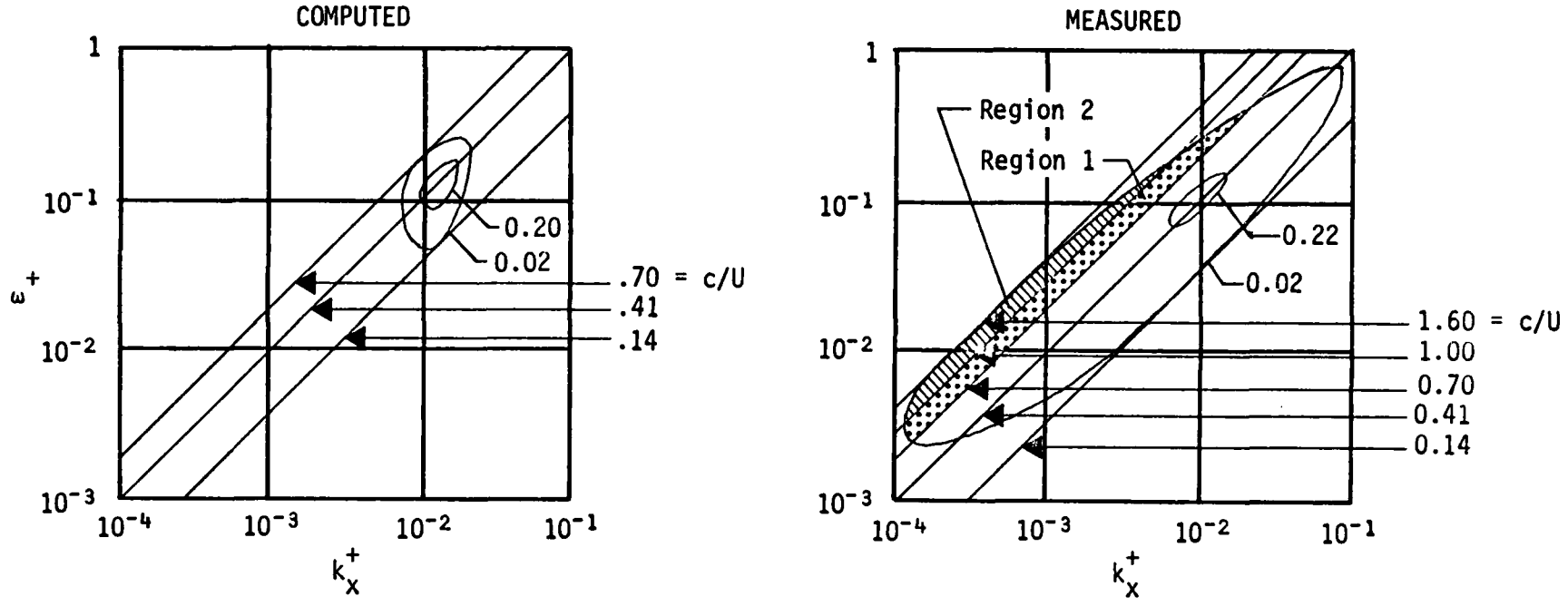

FIGURE 2.9 LINES OF CONSTANT CONVECTION VELOCITY OVERLAID ON THE FREQUENCY-WAVENUMBER SPECTRA OF FIGURE 2.1

NOTE: Only two constant power density contours are reproduced.

The task of analytically predicting the relative contributions of continuum modes, discrete modes and their interactions is conceptually straightforward but quite laborious. Three steps are involved, namely: 1) the determination of the three-dimensional continuum by numerical solutions of the Orr-Sommerfeld equation; 2) the extension of Bark's linear response calculations to include the continuum contribution in the context exemplified by Equation (10) of Section 2.2; 3) the assessment of the three-way nonlinear interactions among finite amplitude discrete modes, finite amplitude continuum modes and the mean flow. None of these steps has been pursued in previous studies. The effort required for their execution certainly exceeds the limited resources available under the present contract. Also, the effectiveness of a strictly analytical approach vis a vis a selective combination of theory and experiments is not obvious at this early stage of the program. Thus, our case rests on the bridging arguments presented heretofore and below.

The asymptotic behavior of the continuum eigenfunctions displayed in Equation (14) provides the basis for some additional observations. Clearly the first term at the right hand side of (14) represents a wave traveling away from the body with wavevector $\underline{k}_t$ of modulus $|\underline{k}_t| = \{[Re(k)]^2 + m^2\}^{1/2}$ inclined at an angle $\theta = \tan^{-1}[m/Re(k)]$ with respect to the x-axis. The second term represents a wave traveling toward the solid boundary with complex amplitude B, wavevector of modulus $|\underline{k}_t|$ inclined at the angle $-\theta$ with respect to the x-axis. Finally, the third term represents a "wall" wave propagating parallel to the solid boundary with complex amplitude C and wavenumber Re(k). In general, the modulus and argument of B and C can only be determined upon calculation of the eigenfunctions and matching of the two wall boundary conditions; however, preliminary estimates indicate that $|B| \to 1$, $\arg(B) \to \pi$, $|C| \to 0$, $\arg(C) \to (-\pi/2)$ for $\theta \to 0$, i.e., $m \to 0$ and $c \to 1$. These, we submit, are the waves that, upon nonlinear interaction, significantly contribute to the low wavenumber and acoustic components characterized by $(c/U_\infty) > 1$. It is well known (e.g., Bergeron 1973) that the low wavenumber component must decay exponentially with y, the coordinate normal to the wall, while the acoustic component must be periodic in y. Because of their low wavenumbers both components must also be characterized by extremely small damping rates in the propagation direction. Since damping rates add in any nonlinear interaction (whether sum or difference), we require that

$$Im(k_1) + Im(k_2) \lesssim Re(k_1) - Re(k_2)$$

in the interactions between $Re(k_1)$ and $Re(k_2) \simeq Re(k_1)$ which yield the low wavenumber and acoustic components. The requirement is clearly violated by modes with $[Im(k)/Re(k)] = O(1)$ such as the Tollmien-Schlichting modes $[Im(k)/Re(k) \simeq 1/3]$ or the continuum modes with phase velocity measurably different from unity $[Im(k)/Re(k) \simeq (1 - c)^{1/2}]$. By contrast, if we restrict attention to interactions between continuum modes characterized by $\Theta \rightarrow 0$, we recover the low wavenumber component by considering pairs such that

$$C_1 C_2^* \exp\{-[Re(k_1) + Re(k_2)]y\} \exp[i(k_1 - k_2)x] + c.c. >> \{B_2^* \exp[i(m_1 + m_2)y] + B_1 \exp[-i(m_1 + m_2)y] + \exp[i(m_1 - m_2)y] + B_1 B_2^* \exp[-i(m_1 - m_2)y]\} \exp[i(k_1 - k_2)x] + c.c. \quad (15)$$

as $y \rightarrow \infty$, and we recover the acoustic component by considering pairs for which the inequality (15) is reversed. Since preliminary estimates indicate that C becomes comparable to B for $\Theta \simeq 10^\circ$, while $C << B$ for $\Theta \rightarrow 0$ (as noted above), we attribute the generation of the low wavenumber component to interactions among pairs with $\Theta \simeq 10^\circ$ and the generation of the acoustic components to pairs with $\Theta \rightarrow 0$. Preliminary consideration of compressibility effects -- which must be recognized when the phase velocity of the difference modes approaches sonic -- suggests that the y-damping of the C components is reduced and, thus, the inequality (15) attendant to low wavenumbers may be satisfied by values of Θ even smaller than the 10° noted above. This finding is exploited in Section 3.0 to select outer decoupler designs that reject waves incident at $\Theta \lesssim 10^\circ$.

The recovery of the proper asymptotic ($y \rightarrow \infty$) behavior for the low wavenumber and acoustic components of the spectra on a mechanistic basis, although conceptually satisfying, does not constitute the ultimate test for the views here presented. Recent models of jet noise associate the acoustic radiation with a specific aspect of turbulence dynamics, viz, the jitter of the large scale coherent motions. The question then arises as to whether the jitter does reflect nonlinear interactions between continuum and discrete modes that are excited to significant levels according to the evidence presented above. The matter is discussed in the following paragraph.

2.5 WAVE RADIATION DUE TO JITTER OF TBL COHERENT MOTIONS

Ffowcs-Williams and Kempton (1978) have assessed the importance of the coherent large scale motions in a turbulent jet as a source of noise. They conclude that those motions provide the dominant contribution by way of the randomly jittering process of eddy coalescence which is responsible for the smooth growth of the jet in the mean. The vortex-pairing model, which fairly predicts the experimentally observed characteristics of excited jets as well as the attendant overall sound intensity, indicates that the magnitude of the radiated sound is determined by the eddy strength but the spectrum is controlled by the randomness in the position of pairing. If the variation in the random position of pairing g(t) is small compared to the scale k_0^{-1} of the eddy, i.e., if $\langle g^2 \rangle k_0^2 \ll 1$, sound is radiated only at certain discrete frequencies; by contrast, if $\langle g^2 \rangle k_0^2 \gg 1$, the radiated sound is broadband with spectral width directly proportional to $\langle g^2 \rangle^{1/2} k_0$ and inversely proportional to T_g, the correlation time of the randomness. Since smooth mean flow growth requires that the position of pairing vary over a distance comparable to the eddy separation, the condition $\langle g^2 \rangle k_0^2 \gg 1$ applies with attendant implications for the acoustic radiation.

In Section 2.4 we have suggested that interactions among continuum modes having finite amplitude (see Figure 2.9) and convection velocity $c \to 1$ are responsible for the acoustic radiation. In view of Ffowcs-Williams and Kempton's result we infer that the same modes must also be responsible for the jitter of the large scale coherent motions associated with the spectral peak discrete (Tollmien-Schlichting) modes. In that connection we note that, due to their finite amplitude, the considered continuum modes can measurably distort the mean flow much as the discrete modes do (see Vaglio-Laurin and Liu, 1981, for a particular example of such distortion). The longer life (smaller damping rate) of the continuum modes can compensate for their lower amplitude vis a vis that of the discrete modes to yield comparable intrinsically unstable, inflectional distortions of the mean velocity profile which, in turn, lead to a burst. However, due to the different phase velocities and damping rates of the continuum and discrete modes ($c \simeq U$ and $c \simeq .4\ U$, respectively), the attendant mean flow distortions exhibit a time dependent, but periodically recurrent, phase relationship. The strength, structure and

space/time separation of the ensuing bursts then display periodically recurrent time dependencies, i.e., jitter. Since the properties (amplitude, wavenumber, frequency) of the mean-flow-distorting, jitter-producing continuum and discrete modes scale with the local boundary layer characteristics (U, δ^*, c_f), we expect that the statistics of the jitter scale with the same quantities. The few available experimental observations confirm this view, at least for what concerns the lowest statistical moments -- i.e., the mean and the standard deviation. With specific regard to the standard deviation (of the jitter) we further expect that it be comparable with the wavelength of the dominant, intracting continuum and discrete modes, i.e., approximately $2\delta \simeq 16\delta^*$ according to Figures 2.1 and 2.9. For smooth mean flow growth we also require this value to be comparable with the mean separation distance d between bursts. The rough equality is supported by the available measurements in that the mean time between bursts, $T \simeq 5(\delta/U_\infty)$, combines with the aforenoted propagation velocity of the energetic Tollmien-Schlichting waves, $c \simeq .4\, U_\infty$, to yield $d \simeq cT \simeq 2\delta$. Thus, the periodically recurrent phase coincidence of continuum/discrete modes with attendant mean flow distortions yields, in principle, a jitter of the coherent motions with low order statistics having the correct order of magnitude and scaling. Only in passing we note that, although the driving mechanisms is deterministic, the jitter can exhibit complex, seemingly random, behavior because a large number of continuum modes (and attendant mean flow distortions) contribute to the process. Evidence to that effect is provided by recent studies of the evolution of non-linear water waves subject to the well-known Benjamin-Feir modulational instability (Yuen and Ferguson, 1978); numerical solutions of the governing cubic Schrödinger equation show that a single wave, initially subject to monchromatic spatial amplitude modulation with wavenumber Δ, evolves in either simple or complex (and seemingly random) fashion depending on whether only the initial modulational perturbation, or the perturbation and several of its harmonics, contribute to the process (Figure 2.10). In either case the initial simple configuration is recovered periodically (Fermi-Pasta-Ulam recurrence).

The quantitative characterization of the jitter of coherent motions in TBL flows has received scant attention even in recent experiments, mainly because measurements are typically performed with a modest number of fixed

(a)

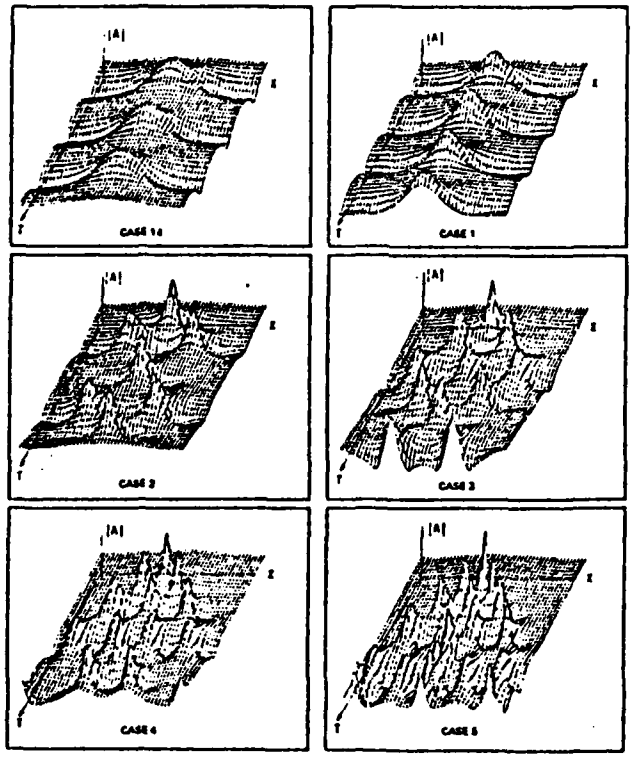

(b)

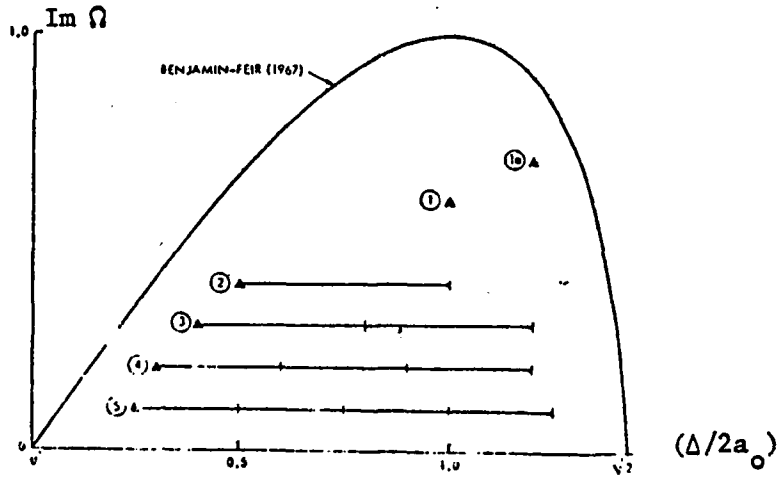

FIGURE 2.10 THE LONG TIME EVOLUTION OF THE ENVELOPE AMPLITUDE |A| FOR A NONLINEAR WAVE SUBJECT TO BENJAMIN-FEIR MODULATIONAL INSTABILITY AND INITIAL CONDITIONS $T = 0$, $A = a_o\ (1-0.1 \cos 2\pi\Delta X)$.

Note: (a) Simple and complex evolutions calculated for different values of the perturbation wavenumber Δ.

(b) Stability map of the normalized perturbation wavenumbers $(\Delta/2a_0)$ used in cases 1a through 5 and their harmonics $(n\Delta/2a_0)$ (from Yuen and Ferguson, 1978).

The complexity of the response at (a) increases as the number of unstable harmonics increases.

point sensors. Thus, we have little evidence to quote except for the results of Dimotakis and Brown (1976), who measured velocity autocorrelation functions near the edges of the mixing layer between two streams having velocity ratio $(U_1/U_2) = 5$. When plotted against the local dimensionless structure lifetime $[\tau U_c/(x-x_o)]$, these autocorrelations retain oscillatory character for time lags much longer than unity (Figure 2.11). The existence of memory times well in excess of the structure lifetime suggests that phase is not completely destroyed in the amalgamation process that erases a structure but, instead, remains coupled to the phase of structures formed subsequently. This long time coupling, as well as the seemingly random jitter observed concurrently, are plausibly explained only by a non-linear interaction between sequential instability wave packets and lightly damped continuum modes excited in the non-linear process of structure formation with simultaneous mean flow and eigenfunction distortions (Vaglio-Laurin and Liu, 1981).

All the above arguments lead to the conceptual reconciliation of the Ffowcs-Williams and Kempton viewpoint (spectral characteristics of the acoustic radiation determined by the low order statistics $\langle g^2 \rangle^{1/2}$, T_g) with the viewpoint of Section 2.4 (spectral characteristics of the acoustic radiation determined by the spectral density of the continuum modes with $c \simeq U$ partaking in the TBL response to a burst). In our mechanistic view the length/time scales and densities associated with the continuum modes in question are uniquely related to those of the dominant discrete modes by the modulation of the attendant eigenfunctions with the shape of the common forcing stress pulse provided by the burst. The length/time scales and power densities associated with interactions between continuum modes -- leading to acoustic radiation -- and with interactions between continuum and discrete modes -- leading to jitter -- are then also in fixed ratios. As a result, the same spectral characteristics of acoustic radiation must follow from the two viewpoints.

The reconciliation above completes the arguments in support of our rudimentary mechanistic view of TBL dynamics and its cause-effect relationships with three components (convective, low wavenumber, acoustic) of wall pressure fluctuation spectra. Some implications of this view for data analysis, scaling and acquisition are discussed in the following paragraphs.

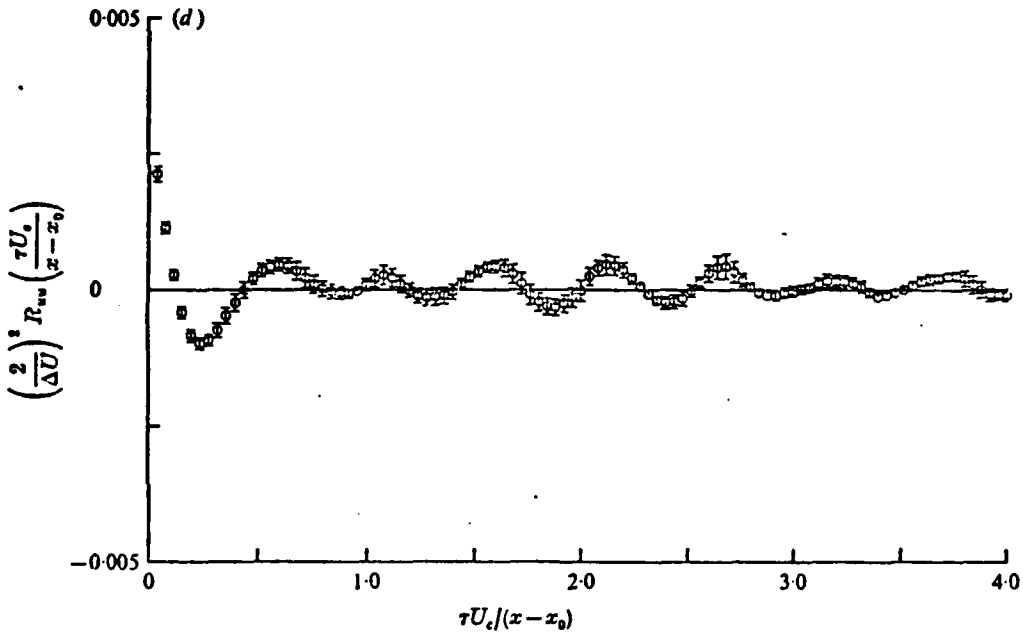

FIGURE 2.11 SCALED VELOCITY AUTOCORRELATION FUNCTIONS
MEASURED NEAR THE EDGES OF A MIXING LAYER
(from Dimotakis and Brown, 1976)

2.6 IMPLICATIONS FOR DATA ANALYSIS AND ACUISITION

In addition to affording a basis for the selection of candidate outer decoupler concepts and a related design approach -- to be elaborated in Section 3.0 of this report -- the considerations of the previous paragraphs are aimed to provide a systematic context for:

- The analysis of data to be acquired under the ACSAS program
- The integration of those data into well founded, working, mathematical models of low wavenumber wall pressure fluctuations and their parametric sensitivities.

The potentially useful role of the mechanistic view in support of those objectives is indicated by the following brief comparative discussion of selected field and laboratory data.

Field data indicate that, at the speeds and stations of interest (say $U \geq 5$ m s^{-1}, $x \leq 30$ m), the flow noise in low frequency bands (say one octave bands centered at frequencies $\omega \leq 500$ Hz) varies like $U^7\omega^{-4}$ for a fixed point sensor on board a full scale vehicle. This noise increases rapidly with the location of the sensor along the hull, the doubling distance being roughly three meters. By contrast, the noise measured by a remote sensor varies like U^4.

The contrasting velocity dependencies of the two sets of data indicate that the on board measurements are dominated by the contributions of direct path and hull-transmitted turbulent wall pressure fluctuations and not by the radiated sound that affects the remote sensor. The $U^7\omega^{-4}$ dependence is in fact consistent with the form of the wavevector-frequency spectral density of turbulent wall pressures suggested by several authors (e.g., Blake and Chase, 1971, Chase, 1980), namely

$$P(\underline{k},\omega) = \rho^2 u_*^6\, \omega^{-3}\, F(u_*\underline{k}/\omega,\ \underline{k}\delta,\ \omega\nu/u_*^2) \tag{16}$$

where $u_* = U\sqrt{c_f/2}$ denotes the friction velocity and ν the kinematic viscosity. The same dependence is also consistent with the laboratory measurements of Martin and Leehey (1977) who found

$$P(k_x,\ 0,\ \omega) \propto \rho^2 U^3 \delta^{*3}\ (\omega\delta^*/U)^{-3.34}(k_x\delta^*)^{0.03} \tag{17}$$

Significantly, neither theory (16), nor laboratory experiments (17), give any indication of the rapid noise increase with sensor location along the hull observed in the full scale measurements. The latter effect has been attributed to forward-propagating hull-borne modes that decay by radiation. However, the explanation is not fully satisfying because it implies predominence of the hull-path contribution over the direct-path contribution at all stations $x \leq 30$ m. Thus, some reflection about potential shotcomings of theory and laboratory experiments is in order.

With regard to the theory we note that considerations -- including many presented in earlier paragraphs -- are generally based on the assumption of a spatially homogeneous TBL. In practice the boundary layer is not spatially homogeneous and, therefore, "correlations" depend upon position as well as separation. This fact was recognized by Bergeron (1973) who showed that, on a finite plate of dimension L much larger than an acoustic wavelength λ_a, correlations become position-independent only for points $\underline{x}$, $\underline{x}^1$ characterized by $|\underline{x}-\underline{x}^1| << L$ and by distances $O(L/2)$ from the boundaries (for both $\underline{x}$ and $\underline{x}^1$). Only at such points does the infinite plate spectrum become correct for the finite problem, an exception still being required for a neighborhood $O(\delta^*/L)$ of the acoustic wavenumber $M(\omega\delta^*/U)$. At all other points correlations and spectra are affected by the inhomogeneities of the flow which include: the TBL spatial growth rate; the ratio of the mode wavelength to the distance from the edges of the surface supporting the TBL; the ratio of the mode wavelength to the principal curvatures of the surface supporting the TBL. Our mechanistic view provides the context for examining these effects. For example, the TBL spatial growth rate is expected to influence significantly and differentially the amplification rate of the energetic modes, much in the same fashion as flow divergence does in jet flows (Crighton and Gaster, 1976, Fuchs et al., 1979). The proximity of edges -- with attendant spatial variations in the mean flow structure -- is expected to alter measurably the energy content of commensurate low wavenumber modes, even though they may be generated by difference interactions of relatively high wavenumber modes that are per se insensitive to the mean flow variations. Similarly surface curvature must and can readily be recognized in calculations of difference modes with wavelength comparable to the principal radii of curvature simply by casting the problem in the appropriate curvilinear coordinate system, rather

than in the traditional Cartesian reference frame. In this light the effects of spatial inhomogeneities upon the low wavenumber and acoustic components of wall pressure fluctuation spectra can be recognized only if the functional dependence (16) is generalized to the following form based on outer variables*

$$P(\underline{x},\underline{k},\omega) = \rho^2 U^6\, \omega^{-3}\, F[U\,\underline{k}/\omega,\ \omega\delta^*/U,\ c_f,\ M,\ \underline{k}\cdot\underline{d},\ \underline{k}\cdot\underline{i}_1\, R_1,$$

$$R_2/R_1,\ \delta^*\,\nabla(p/\rho U^2)] \qquad (18)$$

In (18) c_f denotes the skin friction coefficient, M the outer flow Mach number, and $\underline{d}$ the vector distance between the observation point $\underline{x}$ and either the surface edges or the boundary layer origin; $\underline{i}_1$ is the unit vector in one of the directions of principal curvature and R_1 the attendant radius of curvature; R_2 is the second radius of principal curvature and $\delta^*\nabla(p/\rho U^2)$ the dimensionless pressure gradient.

The drastic escalation in the number of parameters appearing in (18) vis a vis (16) cannot be rejected a priori as a frivolous academic exercise, devoid of practical impact and, therefore, unworthy of careful consideration. In that regard we pause to calculate the parameter combination

$$(Uk/\omega)^{-1}\, M(kd) = k_{ac}(\omega)\, d$$

for the median conditions of the Martin and Leehey (1977) experiment. According to the findings of Bergeron (1973) -- already quoted above -- the product $k_{ac}d$ must be much larger than unity if the infinite plate spectrum is to be recovered on a finite size plate. However, with $U \simeq 40$ m s^{-1}, $M \simeq .13$, $\delta^* \simeq .5$ cm, $k\delta^* \simeq .5$, $(\omega\delta^*/U\infty) \simeq 2$, $d \simeq 35$ cm (equal to the radius of the bass drum frame which in our reading of Martin and Leehey's sketches represented the largest dimension for the test fixture in the free jet facility), we calculate $k_{ac}d \simeq 1.85$ in apparent violation of the Bergeron requirement. We then become concerned upon the impact of the indicated nonhomogeneity upon the data and upon their unexplained 10 dB difference vis a vis the results of Jameson (1975) in a similar experiment. We cannot settle the issue because

---

* According to the mechanistic view set forth in previous paragraphs the significant modes scale with outer variables.

parametric dependencies of the spectra upon spatial inhomogeneities are unknown at present. However, we submit that the large disparity between the two sets of measurements has such practical significance as to warrant investigation of the matter in forthcoming ACSAS studies.

As in Section 2.5 we take the view that, at this stage of the program, the issue of flow inhomogeneities and their influence upon wall pressure fluctuation spectra is best approached by a combination of:

- Theoretical model solutions quantifying specific individual effects.
- Data analyses seeking to recognize those effects and their interplays in the data to be acquired under the ACSAS program.

We outlined approaches to some theoretical problems when we first mentioned TBL growth rate, surface curvatures, etc., as factors. With regard to the data analysis we suggest that valuable information may be gained from comparative studies of space/time correlations obtained at different spatial locations on a given model and/or on different models whose goemetries cover significant ranges of the parameters listed in (19). Admittedly the suggestion is rather imprecise, but we have not had the opportunity to study the model configuration and instrumentation layout being planned for the forthcoming field experiments.

We close with a note on data acquisition in possible laboratory experiments. The difficulty of wall pressure fluctuations measurements at low wavenumbers is well recognized and the susceptibility to contamination by facility acoustic background is well known. According to the wavemechanical view of this report the difficulty stems from the fact that the continuum eigenfunctions -- which govern the generation of the low wavenumber and acoustic components of the spectra -- tend to zero as the wall ($y = 0$) is approached. By contrast, those eigenfunctions oscillate with constant, finite amplitude outside the boundary layer ($y \to \infty$), where the energetic Tollmien-Schlichting modes decay exponentially. Measurements just outside the boundary layer should then considerably enhance the detectability and diagnostics of continuum modes and their derivative low-wavenumber as well as acoustic modes. The observations of Dimotakis and Brown (1976) quoted in Section 2.5 were made

possible by just this approach: the identical, long-persisting velocity autocorrelations (Figure 2.11) detected near the two edges of the shear layer could hardly be recoved within the shear layer due to the high level of small scale turbulent activity prevailing there. Should laboratory experiments prove desirable in the ACSAS program, the approach may be used in conjunction with the heated model design suggested by Vaglio-Laurin, Hoglund and Collier (1982) to facilitate the quantification and subtraction of background acoustic noise.

3.0 OUTER DECOUPLER DESIGN APPROACH

In this section of the Report we concentrate on those features of outer decoupler design which are relevant to signal transmission and flow noise isolation. With respect to the former, we clearly wish to receive the desired signal within a specified range of fidelity. With respect to flow noise, we wish to reduce it to levels equivalent to the ambient noise of the sea. We shall also find that the outer decoupler affects the reception of self noise, and we shall make some extensions of our work to include this as well.

The outer decoupler can be seen as a layer of polymeric material supported in some manner by the base structure. We assume that this layer is not covered with a structural skin but extensions to such a domed structure would be straightforward.

All the essential properties of the outer decoupler layer and its support structure can be made evident by the analyses to be presented here. At this point our effort is less to settle on a particular design and more to put forth an approach by which a detailed design could be carried forward. Also these analyses are intended to help guide test programs which no doubt will be part of the development.

3.1 TWO-DIMENSIONAL MODEL FOR SIGNAL RESPONSE

We consider first a flat layer upon which is incident the signal. (To the extent we are dealing with acoustic ambient noise and/or acoustic self

noise, as in surface reflected signals from the engine compartment, noise properties will be identical.) This 2D layer is taken first to be a fluid with zero internal dissipation. In this Report we consider the base of the layer as an immobile foundation, that is, one of infinite impedance, which could be modified later should the hydrophone designers recommend otherwise.

Figure 3.1 depicts the geometry of the various waves. For harmonic time dependence the equations describing these waves are:

$$\begin{aligned} p_i &= e^{ik_w(x\cos\theta + z\sin\theta)} \\ p_r &= \mu_r e^{ik_w(x\cos\theta - z\sin\theta)} \\ p_t &= 2\mu_t \cos k_L(z - h)\sin\theta_t \; e^{ik_L x \cos\theta_t} \end{aligned} \tag{1}$$

where p_r and p_t are the reflected and transmitted waves resulting from the incident pressure p_i, μ_r and μ_t are reflection and transmission coefficients, k_w and k_L are water and layer wavenumbers, h is the layer thickness, x and z are the coordinates parallel and normal to the layer, and θ and θ_t are the angles of the incident and transmitted waves. We have explicitly shown the reflection and incident angles as equal. Also in these equations we have written p_t as a standing wave, recognizing that it is made up of two travelling waves, i.e., that to get good transmission we must avoid evanescent waves in the layer.

3.1.1 Refraction

We note that the transmitted phase variation in the x direction (which will be used for beamforming) must be identical to the phase of the incident wave. This is automatically so, in order for the system of waves portrayed to be matched at the outer surface. Stated differently the x-going phase matching condition

$$k_w \cos\theta = k_L \cos\theta_t$$

or

$$\frac{\cos\theta}{c_w} = \frac{\cos\theta_t}{c_L} \tag{2}$$

with c_w and c_L the phase speeds in the water and layer, is just Snell's Law. Whatever we choose for the speed in the layer will preserve phase information.

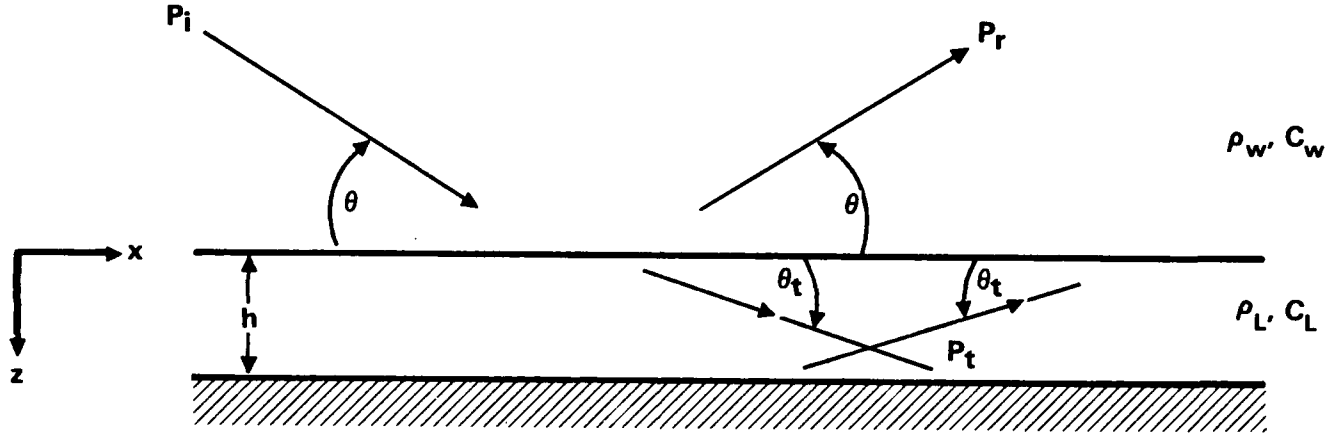

2D Layer and Wave Components

FIGURE 3.1

Our freedom of choice in layer phase speed, however, is not that broad. One limitation for our application is the need to avoid evanescent or exponentially damped waves in the layer. Thus $\cos\theta_t$ must be ≤ 1 for all θ of interest, i.e., the index of refraction n ($\equiv c_w/c_L$) must be

$$n \geq \cos\theta \tag{3}$$

It is useful to introduce the relative speed increase in the layer, Δ. Condition (3) then becomes

$$n = \frac{1}{1+\Delta} \geq \cos\theta \tag{4}$$

Thus the speed can be taken to be less than that of water ($-1 \leq \Delta \leq 0$) so as to satisfy (3) or (4) for all θ. We shall find, however, that slow layers are unsatisfactory from other viewpoints, and we should consider fast ones. We could choose a layer that is at least slightly fast provided we are willing to forego some small angular range $0 \leq \theta \leq \theta_{min}$ wherein (1) is not applicable and instead the input suffers an exponential decay into the decoupler layer. Then we have for the allowable range in speed

$$-1 \leq \Delta \leq \theta_{min}^2/2 \tag{5}$$

where we have taken θ_{min} to be a small angle.

In summary to this point we have found a condition on the sound speed change in the layer and noted that a fast layer can properly be only slightly so.

3.1.2 Transmission

Equation (1) can readily be solved for the ratio of the signal level at the base to the incident signal level. We can define this as the signal gain G and the result is

$$G = \left.\frac{p_t^2}{p_i^2}\right|_{z=h} = \frac{4}{\cos^2(k_L h\sin\theta_t) + \frac{n^2\sin^2\theta}{m^2\sin^2\theta}t\,\sin^2(k_L h\sin\theta_t)} \tag{6}$$

where m is the index of density defined by

$$m = \frac{\rho_L}{\rho_w} = 1 + k$$

with k the relative density increase, and where Θ_t can be found from Equation (2). For the thickness h = 0 we see the gain is 4 (6 dB) as is expected at an immobile foundation. More generally, to avoid rapid oscillations in the frequency response of the layer, the thickness should be made small compared to wavelength in the layer. That is, we must have

$$\boxed{k_L^2 h^2 << 1} \tag{7}$$

Since thickness ultimately will prove valuable as a reducer of flow noise, condition (7) can be seen as restrictive. Put differently, we are forced to have the speed in the layer as high as feasible to avoid undue constraints on thickness.

Coupled with the comments in Section 3.1, one can sense immediately that the applicable design range for sound speed in the layer is governed by

$$\boxed{0 \leq \Delta \leq \Theta_{min}^2/2} \tag{8}$$

This insures fast layers, but only slightly fast, depending upon one's choice of Θ_{min}.

With application of condition (7) the signal gain can be written as

$$G = \frac{4}{1 + (k_L h \sin\Theta_t)^2 \left[\frac{n^2 \sin^2\Theta_t}{m^2 \sin^2\Theta} - 1\right]} \tag{9}$$

This shows that the layer density ideally should be large, i.e.,

$$m^2 >> \frac{n^2 \sin^2\Theta_t}{\sin^2\Theta} \tag{10}$$

which would guarantee that G > 4. But as a practical matter virtually any reasonable choice of m would lead to G $\approx$ 4, and we can relax condition (10).

3.2 A NAVAL-ARCHITECTURAL CRITERION

What is a reasonable choice for m? Clearly ship design and performance would be served if we require the bulk modulus of the layer to be equal to that of sea water. Then compressive strains at depth would be no more in the layer than in water, and concerns usually associated with depth effects evaporate. Thus we take

$$\rho_L c_L^2 = \rho_W c_W^2$$

$$\text{or} \quad m = n^2 \tag{11}$$

$$\text{or} \quad 1 + k = (1+\Delta)^{-2}$$

as the appropriate (reasonable) choice for m.

Equation (8) gives a design range for Δ which, based on the presumption that Θ_{min} and hence Δ is small, leads to

$$\boxed{k \approx -2\Delta} \tag{12}$$

We see that choosing Δ positive (fast layer) leads to a choice of k negative (buoyant layer), an advantage quite apart from acoustic considerations.

Of course slight deviations might be entertained, but to help fix the design approach we settle on Equation (12) as a design constraint.

3.3 THREE-DIMENSIONAL EFFECTS

A 2D layer can hardly be considered a practical model. At minimum the layer is finite and must be structurally supported along its lateral dimensions. Thus we include here an analysis of the effects of finiteness and of lateral supports. We imagine the supports to form some pattern of crossing structural elements as shown in Figure 3.2. These elements define an unsupported layer of area S and perimeter P. Waves within the layer incident on one of these support elements, also shown in Figure 3.2, reflect with an angle β equal to the incident angle. We characterize the reflection with an energy coefficient γ and phase ξ. We also assign a volumetric energy absorption α to the layer material.

For finite 2D bodies, it is well known that the mean free path is S/P where by mean free path we mean the distance averaged over all between successive interactions of the wave with the lateral boundaries. In our case the mean free path is

$$\boxed{r = \frac{\pi S}{p\cos\Theta_t}} \tag{13}$$

which accounts for the up and down travel in the z direction.

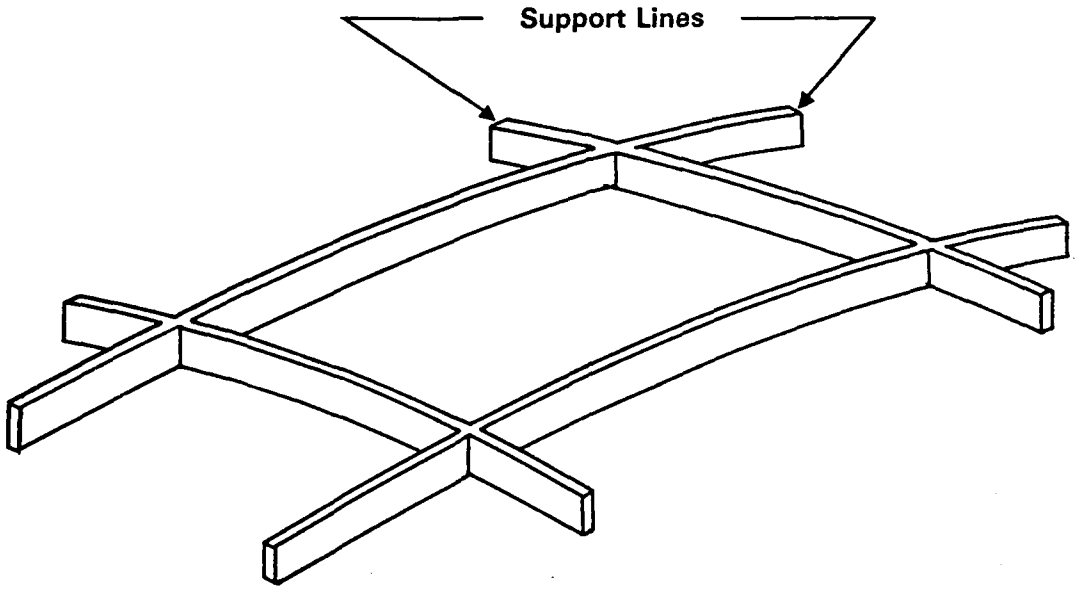

Support Grid
Panel Area: S, Panel Perimeter P

Plan View of Panels and Support Lines

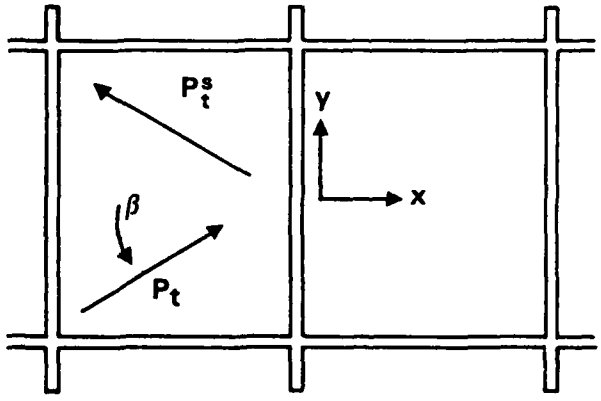

FIGURE 3.2

Each wave within the layer which reflects from one of the support elements can interfere with the incident wave in the layer thereby causing signal confusion. We wish to establish criteria to keep such confusion within acceptable bounds.

Before proceeding, note that we have adopted a forwardscatter or reflection model for the interaction of the layer wave with the support structure. This is justified at least for present purposes by the notion that the individual support elements are likely to be organized along a particular line, the whole of which yields maximum energy in the forward scatter direction.

The wave in the layer incident on a support line is

$$p_t = f(z)e^{ik_L\cos\Theta_t\ (x\cos\beta + y\sin\beta)} \tag{14}$$

where $f(z)$ contains the wave's z dependence. The forward scattered wave is

$$p_t^s = f(z)\gamma^{\frac{1}{2}}e^{i\xi}e^{-\alpha\Gamma/2}e^{ik_L\cos\Theta_t(-x\cos\beta + y\sin\beta)} \tag{15}$$

Aside from the obvious change in direction, the forward scattered wave differs from p_t by containing the support reflection parameters (γ,ξ) and the volumetric attenuation parameter (α). The latter is held to act over a distance covering the mean free path, which merely says that we consider much longer absorption distances as impractical from a signal fidelity viewpoint, and much shorter as implying impractically high attenuation.

The sum of the two interfering signals can be written as

$$p_t + p_t^s = p_t\left[Ae^{i\psi}\right] \tag{16}$$

where the amplitude deviation associated with the layer support structure $(|A| - 1)$ can be found from

$$A^2 = 1 + 2\gamma^{\frac{1}{2}}e^{-\alpha\Gamma/2}\cos(2k_L x\cos\Theta_t\cos\beta - \xi) + \gamma e^{-\alpha\Gamma} \tag{17}$$

and where the phase deviation is

$$\psi = \tan^{-1}\frac{\gamma^{\frac{1}{2}}e^{-\alpha\Gamma/2}\sin(2k_L x\cos\Theta_t\cos\beta - \xi)}{1 + \gamma^{\frac{1}{2}}e^{-\alpha\Gamma/2}\cos(2k_L x\cos\Theta_t\cos\beta - \xi)} \tag{18}$$

We see that both $(|A| - 1)$ and ψ tend to zero with

$$\gamma e^{-\alpha\Gamma} << 1 \tag{19}$$

and this then becomes the relevant condition for design of the support structure. Under this condition we have

$$\boxed{\begin{aligned} |A| - 1 &\approx \gamma^{\frac{1}{2}} e^{-\alpha\Gamma/2} \cos(2k_L x \cos\theta_t \cos\beta - \xi) \\ \psi &\approx \gamma^{\frac{1}{2}} e^{-\alpha\Gamma/2} \sin(2k_L x \cos\theta_t \cos\beta - \xi) \end{aligned}} \tag{20}$$

from which we find the amplitude of the combined signal is practically identical to the desired incident signal. On the other hand, the phase error, while of the same magnitude, may well be non-negligible. We observe this error to be sinusoidal in space; what is of interest is its modulus or maximum value ψ_{max}. We have plotted this in Figure 3.3, and observe that if we wish to keep this error small, mutual conditions are placed on the support absorption parameter γ and the volumetric absorption α.

In subsequent sections of this Report we shall return to some possible choices for these parameters. We do observe here, however, that the energy absorption coefficient can be significantly less than one if the support lines are not solid or do not fully occupy the layer height h. That is, we need not consider support elements with intrinsic sound absorption; they may merely be partial sound transmitters (poor reflectors). We also note that the volumetric absorption can be composed of true polymeric losses in the layer or may be governed by waveguide leakage from the layer; we treat this explicitly in the next Section.

3.4 LOSS FACTOR AND WAVEGUIDE LEAKAGE

The volumetric absorption can be decomposed via

$$\boxed{\alpha = \eta k_L + \alpha_s} \tag{21}$$

where η is the layer loss factor (ratio of imaginary to real part of bulk modulus) and α_s represents equivalent loss associated with waveguide leakage. Loss factor is an important material property; more will be said about it in a subsequent design example. Waveguide leakage is no less important and we now proceed to quantify it.

Figure 3.4 sketches the ray pattern associated with support induced forward-scattered wave in the layer. It executes a complete cycle in a lateral

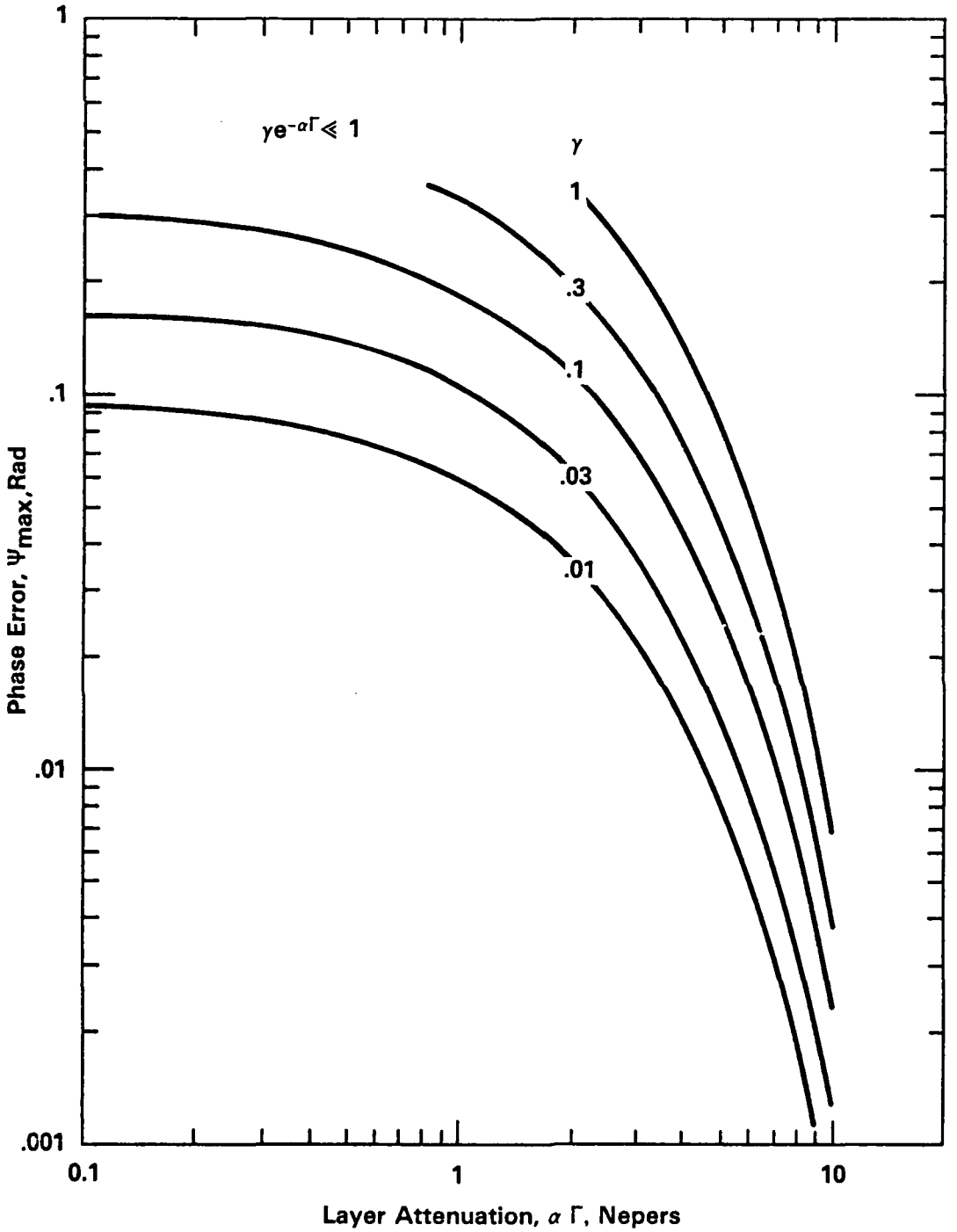
1
.1
.01
.001
0.1
1
10
$\gamma e^{-\alpha\Gamma} \ll 1$
γ
1
.3
.1
.03
.01
Phase Error, Ψ_{max}, Rad
Layer Attenuation, $\alpha\ \Gamma$, Nepers

FIGURE 3.3

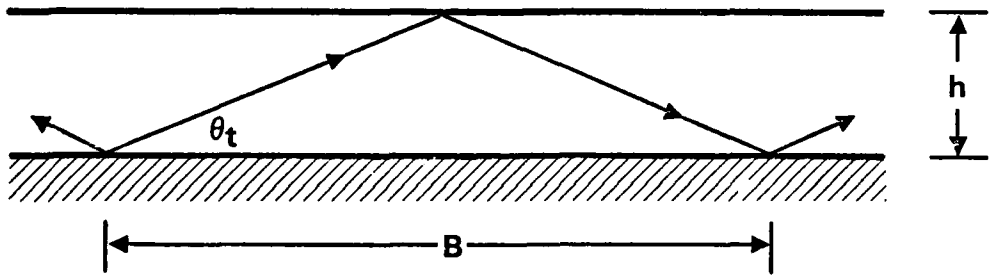

Cycle Distance in Layers

FIGURE 3.4

distance given by

$$B = \frac{2h}{\tan \theta_t} \tag{22}$$

during which it reflects from the water interface once. If the wave reflects weakly (transmits into the water strongly) then it suffers an equivalent volumetric loss, and the layer or waveguide is said to be leaky.

We can write the energy leakage loss for one cycle as $\exp(\xi)$. Then the energy loss in volumetric distance Γ is

$$e^{-\alpha_s \Gamma} = e^{-\xi\left(\frac{\Gamma \cos\theta_t}{B}\right)} \tag{23}$$

under the approximation that the above continuous function represents, on average, the discrete process implied by Figure 3.4 and Equation (22). Finally we can find the loss coefficient ξ from

$$\xi = \ell n \frac{1}{\mu^2} \tag{24}$$

where the layer/water energy reflection coefficient is

$$\mu^2 = \frac{\frac{1}{m}\sin\theta_t - \left[\frac{1}{n^2} - \cos^2\theta_t\right]^{1/2}}{\frac{1}{m}\sin\theta_t + \left[\frac{1}{n^2} - \cos^2\theta_t\right]^{1/2}} \tag{25}$$

This comes from consideration of the layer-trapped scattered wave coupled to a wave radiated into the water. Of course the ray angle θ_t, through Equation (2), converts upon radiation to θ, but now in the transverse plane of the scattered wave in the layer.

We see from Equation (24) that the layer must be fast ($n<1$) to have $\mu^2<1$ for all θ_t, confirming the condition stated in Section 3.1. That is fast layers are leaky and provide control for scattered waves. Slow layers are undesirable since they can trap scattered waves by perfect internal reflection.

Combination of Equations (22), (23), (24), and (25) gives the leakage loss

$$\alpha_s h = \sin\theta_t \, \ell n \left| \frac{\frac{1}{n}\sin\theta_t + \left[\frac{1}{n^2} - \cos^2\theta_t\right]^{1/2}}{\frac{1}{n}\sin\theta_t - \left[\frac{1}{n^2} - \cos^2\theta_t\right]^{1/2}} \right| \tag{26}$$

where we have used the design constraint $m = n^2$ (Equation (11)). That is, we include explicitly the requirement that the layer's bulk modulus equals that of water. The leakage loss is plotted in Figure 5 for small values of positive Δ, corresponding to the desired range of slightly fast layers. Here α_s, in dB/unit length is just 4.34 α_s, the latter in nepers/unit length.

We see from Figure 3.5 and Equation (26) that there is an angle of intromission (Brewster's angle) which is $\theta_b \approx \pi/4$ for $\Delta^2 << 1$. For $\theta_t > \theta_b$, the leakage loss is approximately angle independent, and generally high. For $\theta_t < \theta_b$, however, the leakage loss might be low enough to raise some design issues.

To place the design question in context, however, consider that

- the mean free path Γ is generally much larger than h, i.e., that the leakage loss in a panel is Γ/h times that shown in Figure 3.5
- the loss factor equivalent to leakage loss is

$$\eta_e = \frac{\xi \sin\theta_t}{2k_L h}$$

which suggests that leakage loss is apt to be important even for small ξ and θ_t, because $k_L h$ is small.

To add to these general remarks in understanding leakage loss we need to consider some specific design examples, which we do later in this Report.

3.5 SELF-NOISE LEAKAGE FROM THE OUTER DECOUPLER LAYER

Self-noise entering the outer decoupler from acoustic paths in the sea (e.g., reflection from the free surface) will be modified, if at all, in a manner identical to the signal. But self-noise can come into the outer decoupler via structure-borne paths. These paths ultimately involve the support structure of the layer, and possibly also other structures contiguous to the layer such as that holding the hydrophones.

It is not our present purpose to control structure-borne paths as part of the outer decoupler design, although surely a high degree of interaction ultimately should take place between those responsible for these two

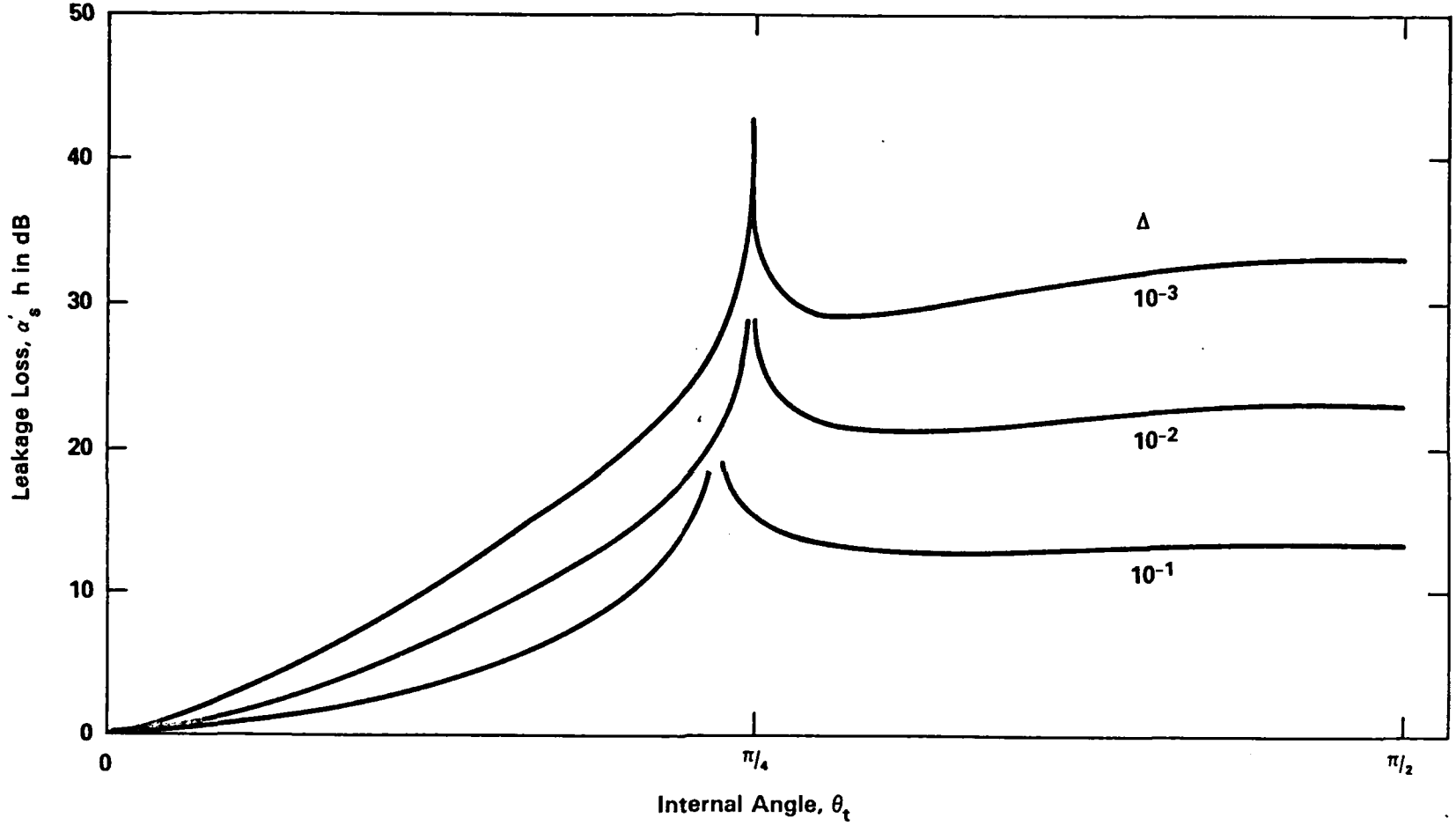
50
40
30
20
10
0
Leakage Loss, α'_s h in dB
Δ
10^{-3}
10^{-2}
10^{-1}
0
$\pi/4$
$\pi/2$
Internal Angle, θ_t

FIGURE 3.5

aspects. What we must do here, however, is assure that such self-noise does not reverberate in the outer decoupler.

The condition placed on structure-borne self noise in the layer follows closely the development of Section 3.3. Since this noise is not correlated with the signal, we merely require its amplitude to be small. Since it is generated at a support structure, its form is just Equation (15). Thus we require

$$\boxed{e^{-\alpha\Gamma} << 1} \tag{27}$$

and this is more restrictive than condition (19). We note, however, that proper attentuation in the structural paths will allow us to use the more moderate one:

$$\gamma e^{-\alpha\Gamma} << 1 \tag{19}$$

3.6 RESPONSE OF THE OUTER DECOUPLER TO TURBULENT BOUNDARY LAYER NOISE

The main thrust in outer decoupler (OD) design for flow noise reduction is to take advantage of the difference in wave-vector characteristics between the desired acoustic field and the undesired turbulent boundary layer (TBL) field. The former has modulus of order $(k_w \cos \Theta)^{-1}$ with general propagation angle Θ between the wave-vector and the solid surface. The latter, based on Part 2 of this report, is characterized by scale of order 2δ (where δ is the boundary layer thickness) and angle $\Theta \simeq 0$ for the dominant wavenumbers associated with the convective ridge, and by larger scale but propagation angle $\Theta < 10^{\circ}$ for the low wavenumbers. The physical description of the turbulent boundary layer forcing function given in Section 2.2 provides a rationale for the design of a decoupler that isolates energy of scale 2δ from the hydrophones and simultaneously reduces the low-wavenumber contributions at near-grazing angles.

We note that the efficacy of the outer decoupler design concepts presented herein is not strictly dependent on the validity of the TBL forcing function description of Part 2. That is, the TBL low wavenumber noise source is either:

1) The nonlinear hydrodynamic interactions of Part 2 that appear at low wavenumber by virtue of high frequency interactions, that enter the outer decoupler at obtuse angles and are rejected along with their high frequency carrier by the scale-selectivity of the OD material, or

2) Acoustic waves of low wavenumber that propagate along the boundary layer waveguide, enter the OD at near-grazing angles and are attenuated by the choice of Θ_{min} as a non-zero small angle.

3.6.1 Scale-selective OD Materials

A homogeneous isotropic material responds to all scales of deformation in accordance with the value of bulk modulus and density. Shear modulus is a parameter also, but only weakly so since it is related to bulk modulus through Poisson's ratio, which would be close to 1/2 for nearly incompressible materials. Such homogeneous isotropic materials offer little advantage as an OD precisely because we need to have it nearly transparent to the acoustic scale, which then makes it also nearly transparent to the TBL scale.

What is needed as an OD is a material with scale-selective elastic properties. In concept such a material would have a modulus at TBL scale much less than that at acoustic scale, and we now proceed to explore its use as an OD. While still homogeneous, the material would be anisotropic to obtain its scale-selective property. We observe that such materials are not oddities and are often used (high transmission-loss architectural panels, optimized noise control mufflers, etc.). They do, however, require special configuration, which materials engineers can readily provide with state-of-the-art technology.

3.6.2 Response to TBL Deformation

Consider a scale-selective material with shear modulus G for TBL scales ($\sim 2\delta$). Consider also that the OD using this material is not too thin, specifically

$$h \sim 2\delta. \tag{28}$$

Then a TBL disturbance at the water interface generates both shear and volume deformations in the OD layer. If the speed of the disturbance at the interface U_c is

$$U_c < C_T \tag{29}$$

where C_T is the transverse (or shear) wave speed [$= (G/\rho_L)^{1/2}$], free surface waves (Rayleigh waves) are generated, and are known to have the form

$$\begin{aligned} \tilde{\Phi} &= \tilde{\Phi}_o e^{ik_T s x}\, e^{-k_T \sqrt{s^2 - d}\, z} \\ \tilde{\Psi} &= \tilde{\Psi}_o e^{ik_T s x}\, e^{-k_T \sqrt{s^2 - 1}\, z} \end{aligned} \tag{30}$$

where $\tilde{\Phi}$ and $\tilde{\Psi}$ are the volume and shear disturbances respectively, x and z are the coordinates parallel to and normal to the layer, k_T is the transverse (shear) wavenumber and

$$s = \frac{c_T}{c_R}$$

$$d = \frac{1 - 2\sigma}{2 - 2\sigma}$$

with c_R the Rayleigh speed and σ Poisson's ratio.

The free surface waves described by Equation (30) attenuate into the layer; this provides the flow noise reduction we seek. To estimate this reduction we need s, which is a function of Poisson's ratio and which has values

σ	0	1/4	1/2
s	1.144	1.088	1.047

These values are not too dependent upon σ and we choose a value corresponding to $\sigma = 1/2$. Then we see that the volume and shear deformations attenuate into the layer with values of about

$$\begin{aligned} &\text{volume:} \quad k_T\sqrt{s^2 - d}\cdot z\ (20 \log e) = 57\ z/\lambda_T,\ \text{dB} \\ &\text{shear:} \quad k_T\sqrt{s^2 - 1}\cdot z\ (20 \log e) = 17\ z/\lambda_T,\ \text{dB} \end{aligned} \tag{31}$$

where λ_T is the transverse wavelength. In the practical case where z/λ_T is large enough to provide useful attenuation, volume deformation can be neglected compared with shear deformation. Since the TBL forcing field is at least as energetic in moment excitation as in force excitation, we may conclude that shear transmission governs flow noise reduction.

Criteria for reduction of flow noise are frequency-dependent. If, however, we satisfy such criteria at the lowest frequency of interest, then in accordance with the foregoing, the noise reduction would increase at the rate of 3 dB per octave, and would likely meet noise reduction requirements for the entire frequency spectrum. With the choise of the lowest frequency as 100 Hz we find, therefore, that we need layer thicknesses as displayed:

Noise Reduction, dB	10	20	30	40
h/c_T, sec. required at 100 Hz	0.59×10^{-2}	1.18×10^{-2}	1.77×10^{-2}	2.35×10^{-2}

We see that c_T must be quite small (say much less than 100 m/sec) to keep h from being impractically large.

3.6.3 Realization of Anisotropic Materials

We sketch in Figure 3.6 a possible configuration for the anisotropic material. This sketch does not exhaust the wide range of material configurations that can be used to achieve our ends, but its inclusion here will help illustrate the design principle.

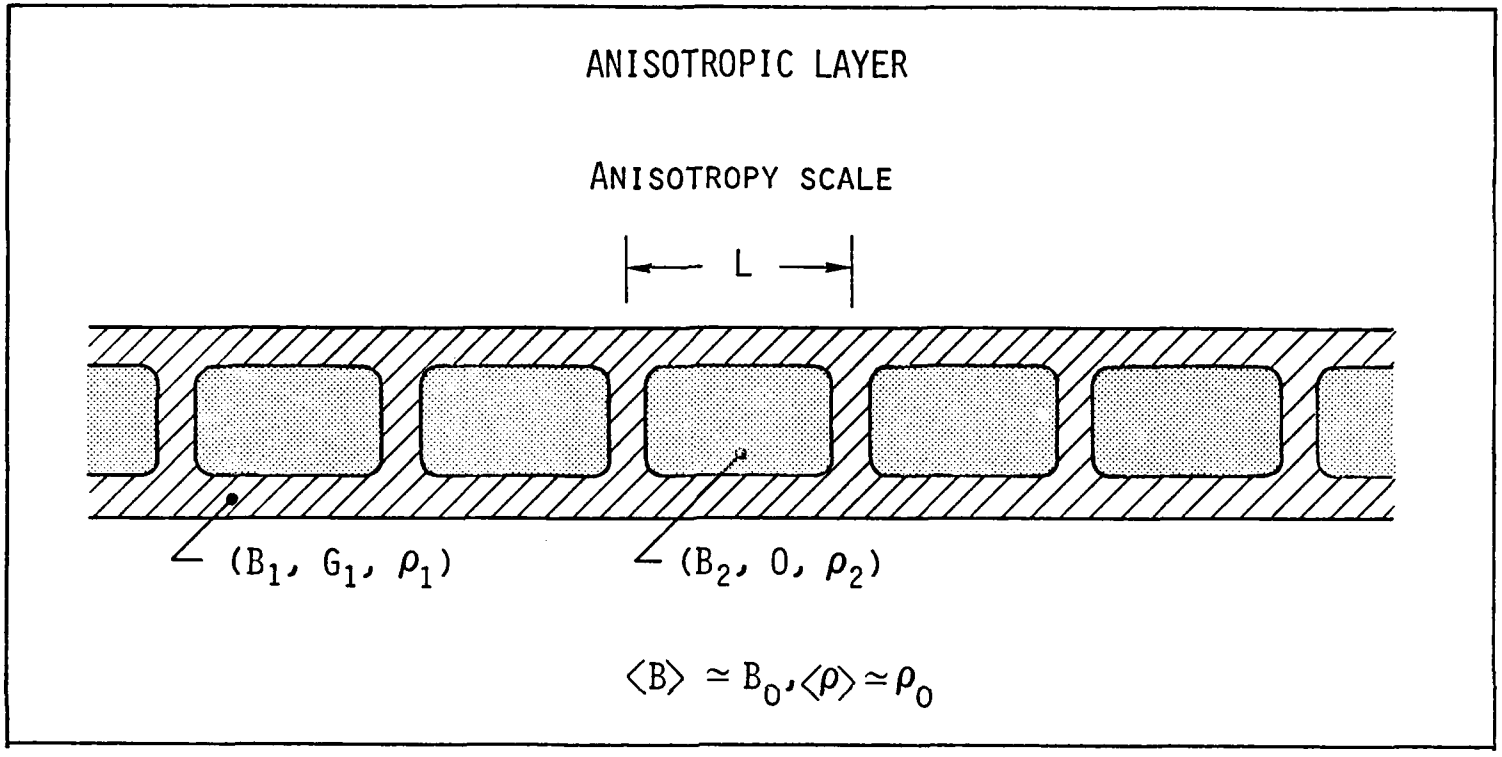
ANISOTROPIC LAYER
ANISOTROPY SCALE
L
(B_1, G_1, ρ_1)
$(B_2, 0, \rho_2)$
$\langle B \rangle \simeq B_0, \langle \rho \rangle \simeq \rho_0$

FIGURE 3.6

Local deformations on the outer surface of the layer tend to buckle the pillars connecting the upper and lower skins. This provides small shear modulus at small scale. At larger scale, however, the pillars do not buckle, given that the volume between them is filled with a liquid-like material. Thus for acoustic scales the large area properties of the layer can be adjusted to have the appropriate c_L. Since the desired c_L at acoustic scale is 1500 m/sec and the desired c_T at TBL is <100 m/sec, we conclude that the materials problem is to design one with bulk modulus to shear modulus ratio more than about 225 (in contrast to isotropic materials with ratios of about 2 to 3). This is a realizable requirement.

3.6.4 Response to TBL Low Wavenumber Components

There is concern that TBL energy at low wavenumbers can be important, and we analyze its reduction here. By choosing a fast layer ($\Delta \geq 0$) such TBL waves are exponentially attenuated, the reduction R in an OD of thickness h being

$$R = \sqrt{k^2 - k_L^2}\, h\ (20 \log e) = 8.7\, k_L h \sqrt{(c_L/U)^2 - 1}, \text{dB} \qquad (32)$$

where k is the flow noise wavenumber and where U is its phase speed. U generally fills the range

$$U_c \leq U \leq C_w \qquad (33)$$

At the convective ridge ($U = U_c$) we have

$$R = 8.7\, k_c h, \text{ dB}$$

since $k_c >> k_L$. We see that

$$\boxed{k_c^2 h^2 >> 1} \qquad (34)$$

is a design condition for control of low wavenumber flow noise.

To be more specific than condition (34), we need to use the spectral density at low wavenumbers. The ratio of unattenuated to attenuated energy is

$$\int_{k_w}^{k_c} k^q dk \Bigg/ \int_{k_w}^{k_c} k^q \exp\left[-\sqrt{k^2 - k_L^2}\ h\right] dk$$

where k^q is a power law approximation to the spectral dependence. Since uncertainty exists on the precise form of low wavenumber spectral density, we choose two values often suggested ($q = 0$, $q = 2$) to evaluate the ratio:

q	0	2
	$k_c h$	$\frac{k_c^3 h^3}{6}$

This evaluation is approximate, but is quite good for our conditions ($k_c >> k_L$, $k_w \geq k_L$, $k_c^2 h^2 >> 1$). Then the reduction R_q in dB is:

$$\boxed{R_o \approx 10 \log k_c h}$$

$$\boxed{R_2 \approx 30 \log\left(\frac{k_c h}{1.8}\right)} \qquad (35)$$

The foregoing developments (Eqs. 32 through 35) assume implicitly that the transition wavenumber for long waves is of the order 1/h. This transition wavenumber is determined by the specific properties of the selected OD material. Conservative practice suggests use of R_o as the approximate design value. Also many researchers in TBL noise tend to favor $q = 0$ as a better representation of available observations.

As in Equation (31), R_o shows the noise reduction increasing at a rate of 3 dB per frequency octave. Thus satisfaction of noise reduction requirements at the lowest frequency of interest (say 100 Hz) should also meet requirements for the entire spectrum.

3.7 ANOTHER NAVAL-ARCHITECTURAL CRITERION

We have already seen that the transverse wave speed c_T should be larger than U_c, the convection speed of the TBL field. It is well known that a flow field over an elastic layer can damage it when the flow speed equals the relevant free wave speed in the layer. To avoid this we adopt the condition:

$$\boxed{c_R > U_\infty} \qquad (36)$$

where U_∞ is the free stream speed. Since c_R is less than c_T ($c_R = c_T/s$) and U_∞ is more than U_c ($U_c \sim 0.8\, U_\infty$), Equation (36) is more restrictive than Equation (29), and we adopt it for conservative practice.

3.8 A DESIGN EXAMPLE

We do not intend to provide a thorough discussion of design alternatives, but it is instructive to carry out a design example. This will indicate the way in which the foregoing models and concepts may be applied, and will help to make firm the design approach.

We have boxed in the most important equations and conditions of the foregoing sections, to make the example easier to follow. As in any design, there is no unique starting point; the designer ultimately will iterate several times to achieve an appropriate compromise among competing desiderata. All specifications in what follows are fictitious, but represent the kind of input the OD designer needs.

1) Choose Δ positive to avoid perfect internal reflection for scattered waves and self noise. [Equations (8) and (25).]

2) The array is specified to operate to within 0.17 rad (10°) of grazing. Thus $\Theta_{min} = 0.17$ and at most $\Delta = 7.6 \times 10^{-3}$. The layer c_L is thus 11 m/sec faster than that of sea water. [Equation (8).]

3) The OD is specified not to collapse at depth. Thus $k = -1.5 \times 10^{-2}$, i.e., its specific gravity re sea water is less by 1.5 percent. [Equation (12).]

4) The OD is specified to have a controlling flow noise reduction requirement of 12 dB at 100 Hz. Thus $h/c_T = 0.71 \times 10^{-2}$ sec, [Equation (31)], and $k_c h = 16$ [Equation (35).]

5) The array is to withstand a free stream speed of 30 m/sec. Thus take $c_R = 33$ m/sec and $c_T = 35$ m/sec ($\sigma \approx 1/2$). [Condition (36).]

6) From (4) [Equation (31)] and (5), $h = 0.25$ m, based on shear deformation.

7) The array is to perform acoustically up to a free stream speed of 12 m/sec. Thus from (4) [Equation (35)], $h = 0.24$ m. Since this is less than that found in (6), step (6) governs.

8) The highest frequency of interest is specified to be 1000 Hz. Thus $k_L h \leq 1.05$ and condition (7) is violated. (At this point one can iterate to remove the violation, or can explore the ramifications of holding to 1000 Hz and 0.25 m. We assume the ramifications can be tolerated, and proceed.)

9) Signal phase error associated with the support structure is specified to be no more than 0.1 rad. Thus $\psi_{max} = 0.1$, and as one possible design branch, take $\gamma = 0.3$ and $\alpha r = 3.4$. [Figure 3.3 or Equation (20).]

10) The condition for control of self noise, Equation (27), is satisfied by the choice in (9).

11) With $\gamma = 0.3$, the support grid should occupy no more than 30 percent of its transverse area. If more than 30 percent is occupied, sound absorption treatments must be designed into its structure.

12) The structural designer specifies, for the 30 percent structure, a support grid of 1 m X 2 m. Thus we find r and α as listed in the following table. [Equation (13) and step (9).]

θ_t, deg	0	15	30	45	60	75	90
r, m	1.05	1.08	1.21	1.48	2.09	4.05	∞
α, nep/m	3.25	3.14	2.81	2.30	1.62	0.84	0
α_s, nep/m	0	3.24	9.86	27.7	20.7	21.9	22.3
η at 100 Hz	7.76	—	—	—	—	—	—
η at 1000 Hz	0.78	—	—	—	—	—	—

13) With $\Delta = 7.6 \times 10^{-3}$ from step (2) and h = 0.25 m from step (6), obtain α_s as in the foregoing table. [Equation (26) or Figure 3.5.]

14) Leakage from the waveguide meets all absorption requirements except for θ_t small. Find required η (listed in the table) to make up this deficiency. (Since the maximum practical η is about 0.1 from a materials viewpoint, and about the same from a signal transmission viewpoint, we must explore the ramifications of violating our requirements at small θ_t.)

This completes a zero-order design, and iteration would yield compromises that perhaps are more acceptable. Note that the values of Δ and h affect the design most dramatically. Also note that the design yields a materials specification which, symbolically, is:

- density: ρ_L
- large scale bulk modulus: $\rho_L c_L^2$
- small scale shear modulus: $\rho_L c_T^2$
- loss factor: η

4.0 PLAN OF ACTION

4.1 INTRODUCTION

The Plan of Action, which we believe is compatible with the ACSAS Program Plan, is organized in three iterative phases based on our understanding of design and test objectives for two major KAMLOOPS tests in FY83 and FY84 and one series of LSV tests in FY86. The KAMLOOPS FY84 tests are to be augmented by selected component full scale submarine tests. The Phase I effort in FY83 is to be directed to initial tests and evaluation of inner and outer decouplers, polymer hydrophones and effects on noise due to hull discontinuities and roughness. The Phase II effort is directed to optimization and definition of array and hull design parameters; Phase III is concerned primarily with propulsion platform effects on array performance and confirmation of the KAMLOOPS data set.

The Plan of Action described in this section is focused on Phase I objectives. The objectives and plans for Phases II and III are only outlined since detailed plans would, of course, depend on Phase I results. The ACSAS program plan is focused on an experimental approach with KAMLOOPS as the principal test platform. This approach involves major attention to experimental configurations, operating conditions and design of measurements and analysis procedures. In particular, it is important to minimize and control external effects which might excessively contaminate the measurements of design and operational variables. In certain cases, it may be desirable to

introduce controlled diagnostic tests to identify and quantify cause and effect relationships for both the needed design parameters and the external factors affecting the measurements.

In addition, it is recognized that testing of outer decouplers and hull coatings must be carried out in close coordination with hydrophone, inner decoupler and hull structural investigtions. The testing requirements of these associated components will determine, to a large degree, the test configurations and measurements for the outer decouplers. Therefore, the following discussion is restricted to guidelines and general approaches to the experimental plan for evaluation of the outer decoupler.

4.2 FY83 -- MAJOR KAMLOOPS TESTS

The Plan of Action for the FY83 KAMLOOPS tests is organized in six tasks directed to specific objectives.

TASK 1

Determine the physical properties and acoustical characteristics of the array outer decoupler system needed to isolate to a satisfactory degree the pressure field of the turbulent boundary layer from the array.

The design parameters for the outer decoupler are discussed in Section 3. They include the following: sound speed, c_L; shear wave speed, c_T; density, ρ; loss factor, η; volumetric absorption, α; and geometric dimensions including thickness, h. In the aforementioned discussion the range of values for these parameters is established qualitatively. In some cases the design objective is well understood and/or the range of practical values is relatively narrow. On the other hand, there is a need to establish criteria for selected design parameters in terms of both performance sensitivity and practical materials engineering and fabrication constraints.

The initial design and test effort is, therefore, directed to determining the effects of design and construction variables in order to establish criteria for subsequent design optimization. The detailed design and test plan will specifically address criteria with respect to the following characteristics:

- Refraction criteria for the prescribed range of c_L
- Transmission loss for a range of ρ
- Support structure energy reflection loss, γ
- Internal volumetric energy absorption, α
- Material loss factor η
- External wave-guide loss, α_s

The approach to this task is to:

1) Develop and refine the analytical results presented in Section 3.0 of this report as may be needed for specifications.

2) Prepare design guides in the form of design envelopes, charts, and tables.

3) Specify the material properties together with the range of particular design parameters needed to establish parameter sensitivity and optimal characteristics through subsequent development and testing tasks.

TASK 2

Monitor the development of design options for the outer decoupler. The approach to this task involves technical discussions with those tasked to design and fabricate the materials to ensure that requirements defined in Task 1 are properly accounted for in the design process and to assess the impact of engineering compromises and alternatives. The design and fabrication of the test configurations must be compatible with KAMLOOPS installation requirements. Specifically:

1) Determine how and to what degree the variations in the design parameters selected in Task 1 can be incorporated in the detailed material configurations.

2) Assess design/cost trade-offs in the design process.

3) Provide technical reviews during the design/development/ process.

4) Work with material fabrication contractors and incorporate standard material testing procedures to determine basic material properties.

5) Ensure compatability with KAMLOOPS installation requirements.

TASK 3

Determine the effects of discontinuities caused by mounting and attachment requirements on the noise coupling into the array and the hull.

Significant progress has been made in recent years in the development and application of hull coating adhesives. It is possible that the outer decoupler installation requirements can be met by adhesive attachment procedures. On the other hand, practical naval architecture requirements may dictate structural strength members. Structural discontinuities are in important consideration in the design of the outer decoupler system as discussed in Section 3.0. The technical approach is to introduce structural connections into selected outer decoupler samples to represent attachments or active strength members. This is an initial step to assess the relative importance of structural discontinuities on the overall performance of the outer decoupler materials. Specifically:

1) Design test configurations with a structural bracket to retain the material on the hull structure; select the material.

2) Monitor the fabrication of these test samples to ensure its compliance with test objectives.

TASK 4

Experimentally determine the characteristics of outer decouplers and the effects of structural discontinuities on noise coupling into the array and the hull.

The conduct of the outer decoupler testing program will be carried out by DTNSRDC staff with the assistance of selected contractors. Our approach is to provide technical support in the following areas:

1) Assist in the development of the test plan for the outer decoupler testing including instrumentation, procedures and analysis plans.

2) Provide sketches for needed instrumentation including locations and mounting provisions for hydrophones and accelerometers.

3) Recommend diagnostic tests for transfer functions and external factors.

TASK 5

Prepare initial evaluation of outer decoupler materials and assess their potential for noise reduction. Define effects of mounting and attachment structures.

The technical approach is directed to early assessments based on on-line data analysis with comparisons to predicted performance. An early or preliminary evaluation is vital to the planning of Phase II FY84 experiments and to the support of design/fabrication efforts. It is important at this state to assess the outer decoupler in the context of the entire system including inner decoupler, hull coatings, structureborne noise control and other features which effect outer decoupler performance. Specifically:

1) Prepare a Quick-Look Report

2) Participate in analysis of data

3) Review designs and prepare optimized material and design specifications for the outer decoupler system including suggestions for changes in the design of other array components such as the inner decoupler and hull coatings and structureborne noise control features.

4) Prepare design guidelines for mounting and attachments methods.

5) Recommend modifications to FY84 measurement and analysis procedures for evaluation of the outer decoupler system

including suggestions for changes in other array features which reflect interpretation of the data on outer decoupler system properties.

TASK 6

Review, interpret and assess scaling rules for existing and new flow noise data in the context of the mechanistic description of noise sources presented in Section 2.0 of this report.

Data are available from full scale submarines and from KAMLOOPS and other scaled-down vehicles. The scaling and correlation of these data remains an issue, however. Some sort of model is a prerequisite for scaling; existing models are quite broad, they fail to correlate the measured spacial dependencies, and they are short on specific, mechanistic physics. We have attempted a start to fill this void. Our approach in this task then is to:

1) Review existing full-scale and scaled-down flow noise data for consistency with the correlations and relations implicit in ORI's description of low wavenumber noise sources.

2) Assist in the development and review of test plans for KAMLOOPS and/or water tunnel tests that would provide information on flow noise sources and characterization.

3) Assist in the interpretation of new data with emphasis on development and validation of scaling rules.

4.3 TEST CONFIGURATIONS

In this section we discuss some approaches to the design and installation of test sections on KAMLOOPS for initial evaluation. We also set forth recommendations on instrumentation and measurement and analysis requirements.

Figure 4.1 illustrates a basic conceptual approach which involves placing the test sections in a peripheral arrangement so that each one is in contact with essentially the same fully developed turbulent boundary layer flow.

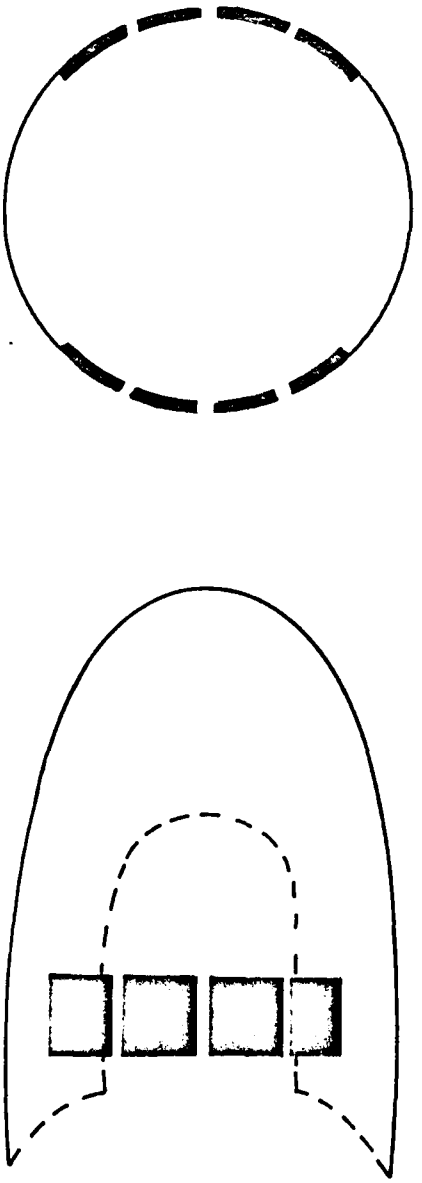

FIGURE 4.1 CONCEPT: LOCATION OF OUTER DECOUPLER TEST SECTIONS ARRANGED PERIPHALLY ON PORT AND STARBOARD BOW AREA, SIDE AND BOW VIEW. FOUR OR MORE ON EACH SIDE.

Figure 4.2 illustrates a second basic conceptual approach which prescribes a common surface geometry for all test sections. This surface would be either a part of the KAMLOOPS bow surface profile such that the test sections would be recessed within the hull lines or parallel to the surface profile such that the test sections would be raised above the hull lines to an equal height. The latter approach requires fairings around the periphery of the hull as shown in the sketch.

Figure 4.3 illustrates a third basic concept, namely that the test sections be structurally isolated from the main hull structures. The effectiveness of the vibration isolation must be established so that the background vibration levels of the hydrophone mounting structures behind the outer decoupler test sections are comparable and below a prescribed acceptable level.

Figure 4.4 shows a suggested arrangement of test sections which involves several "control" sections, i.e., no decoupler, interspersed between the decoupler test sections. These control sections would provide baseline vibration and noise levels under direct TBL pressure field excitation.

Figure 4.5 provides a preliminary concept on measurement requirements. The basic approach is to incorporate both vibration and hydrophone array measurements in order to define the performance of the test sections and isolate the more significant measurement variables and design parameters. An example array for each test section is also shown, consisting of a line array of five hydrophones in both longitudinal and lateral coordinates.

Figure 4.6 shows a preliminary concept for the testing of the effects of structural attachments or strength members.

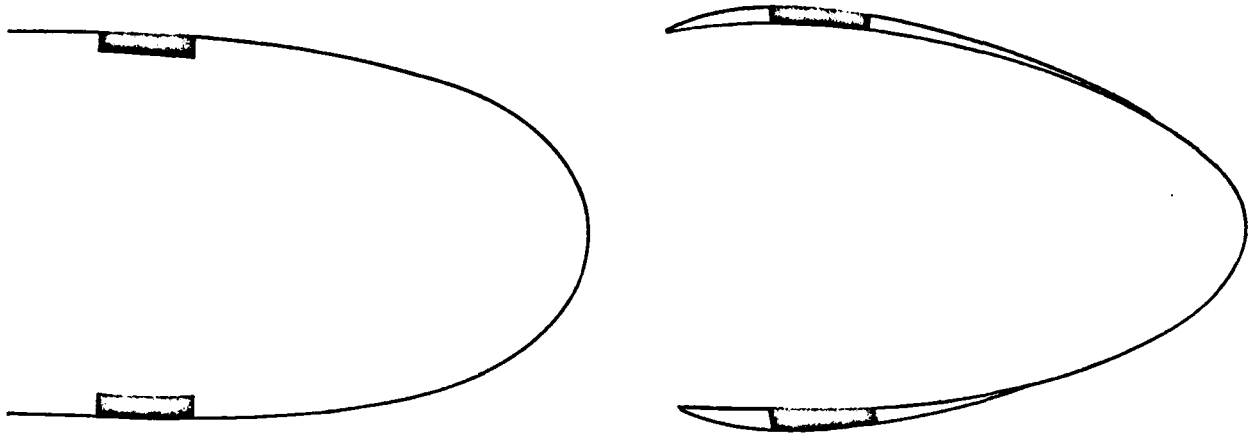

A. Test Section Surface Coincident with Hull Lines

B. Test Sections External to Hull with Fairings

FIGURE 4.2 CONCEPT: PLACEMENT OF OUTER DECOUPLER TEST SECTIONS WITH RESPECT TO HULL LINES - PLAN VIEW

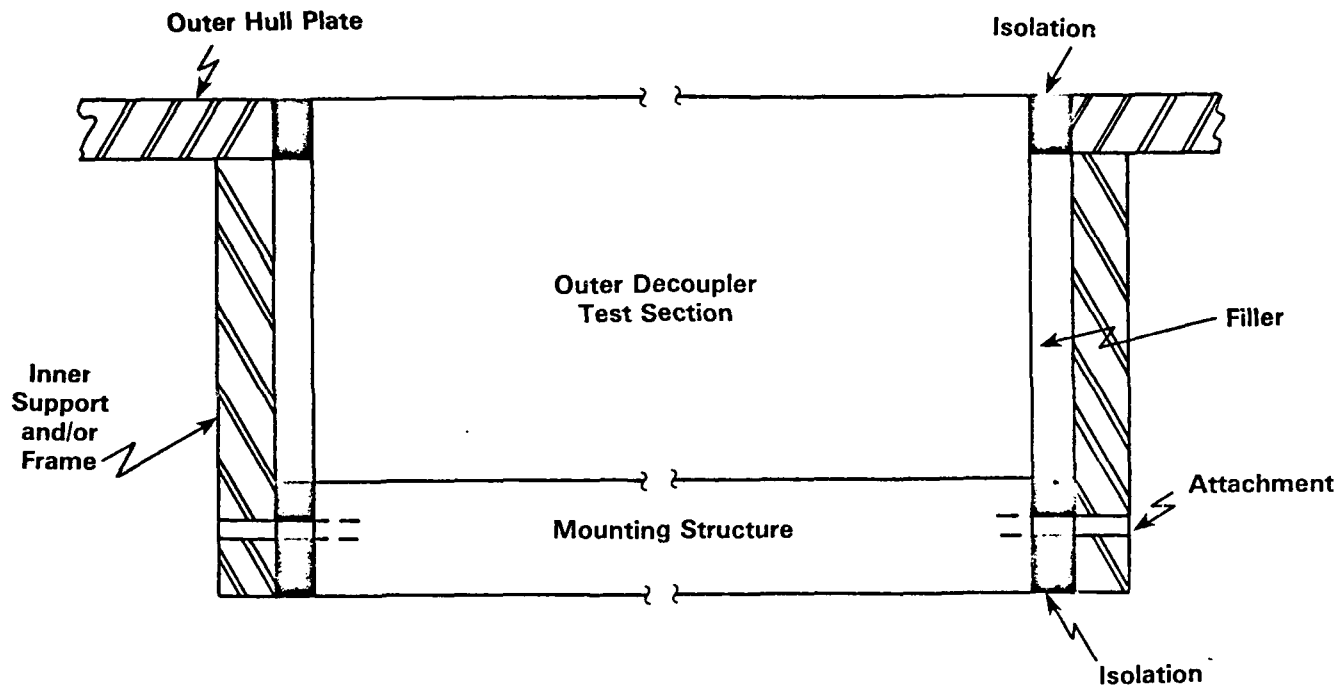

FIGURE 4.3 CONCEPT: INSTALLATION OF OUTER DECOUPLER TEST SECTION; SURFACE COINCIDENT WITH HULL LINES

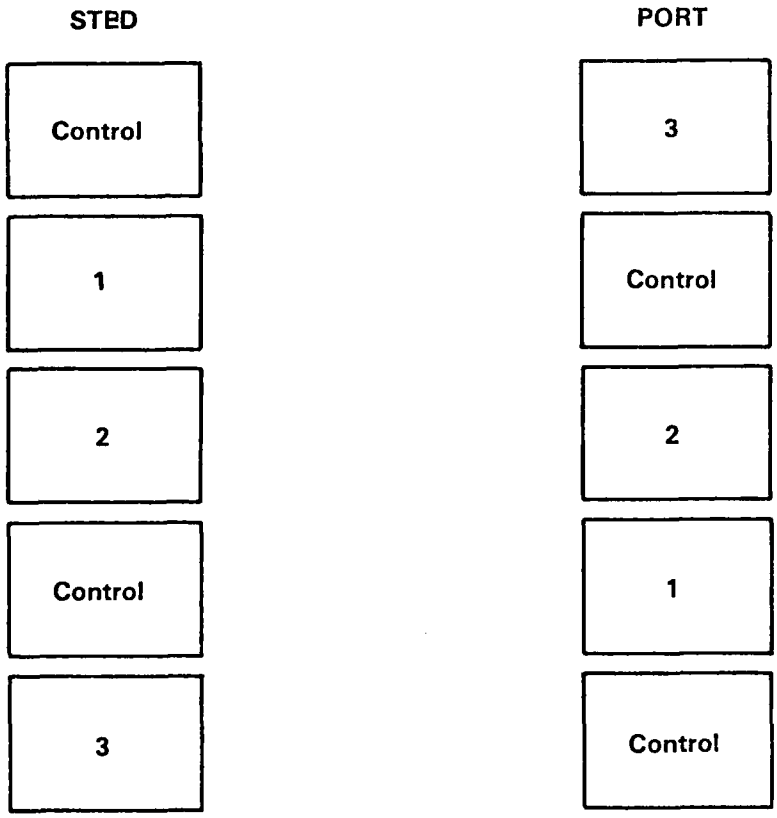

FIGURE 4.4 CONCEPT: ARRANGEMENT OF THREE DIFFERENT TEST SECTIONS WITH SIMILAR CONTROL SECTIONS INTERSPERSED

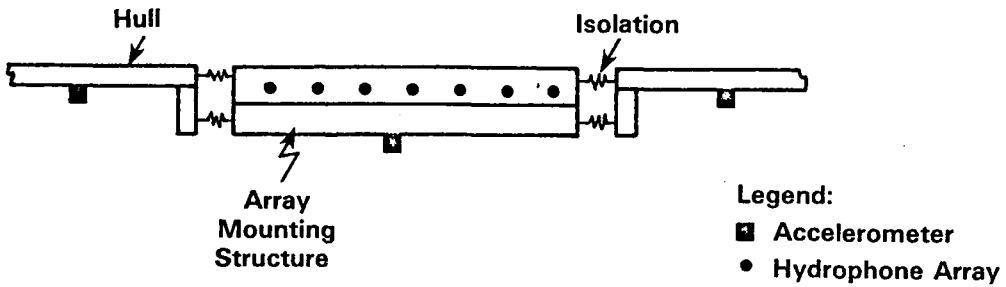

A. Control Configuration — Elev.

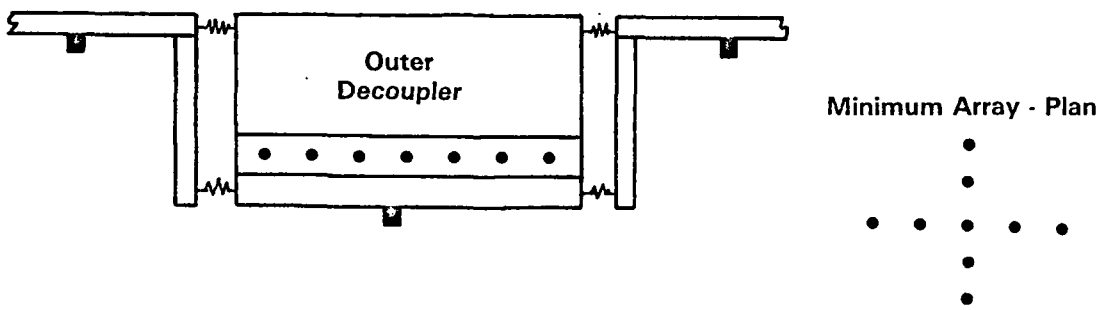

B. O.D. Test Section — Elev.

FIGURE 4.5 SCHEMATIC CONCEPT: MEASUREMENT TYPES AND LOCATION

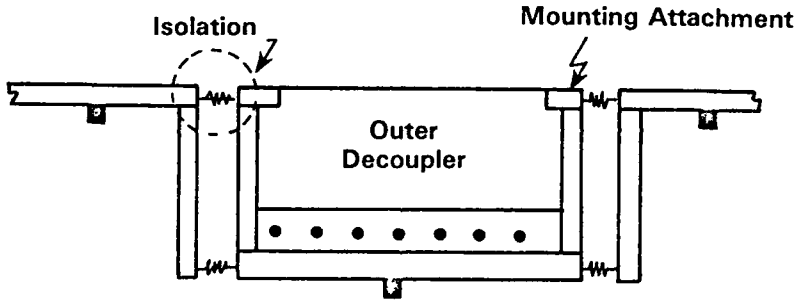

FIGURE 4.6 SCHEMATIC: OUTER DECOUPLER TEST SECTION WITH MOUNTING ATTACHMENT. TEST WITH AND WITHOUT ISOLATION

APPENDIX A

THE DISPERSION RELATION FOR FINITE AMPLITUDE WAVES

For simplicity we consider the nonlinear interactive evolution of a temporally growing (or decaying) finite amplitude two-dimensional wave superposed on the mean incompressible boundary layer flow on a flat plate. We seek to show that one consequence of the nonlinearity is the amplitude dependence of the dispersion relation for the wave.

With reference to cartesian coordinates (x oriented streamwise and y oriented normal to the plate) we assume the initial state of motion to be described by

$$\underline{V}(x,y,0) = [U(y,0) + u(x,y,0),\ v(x,y,0)] \tag{A-1}$$

u and v being periodic with wavenumber k and frequency ω. We determine the temporal evolution of the flow in terms of the stream function $\tilde{\psi}(x,y,t)$ which must satisfy the vorticity conservation equation

$$(\nabla^2\tilde{\psi})_t + \tilde{\psi}_y(\nabla^2\tilde{\psi})_x - \tilde{\psi}_x(\nabla^2\tilde{\psi})_y - \frac{1}{R}\nabla^4\tilde{\psi} = 0 \tag{A-2}$$

where R denotes the Reynolds number formed with the reference velocity U, the reference length δ and the fluid kinematic viscosity ν. We solve (A-2) subject to the initial conditions (A-1) and to the boundary conditions

$$y = 0 \qquad \tilde{\psi} = \tilde{\psi}_y = 0 \tag{A-3a}$$

$$y \to +\infty \qquad \tilde{\psi} \to 0,\ \tilde{\psi}_y \to 0 \tag{A-3b}$$

In seeking the solution we assume that, for all $t > 0$, the stream function $\tilde{\psi}$ may be resolved into a mean flow contribution $\Psi(y,t)$ and a disturbance contribution $\varepsilon\psi(x,y,t)$, the latter possessing small but finite amplitude -- characterized by the parameter $\varepsilon << 1$ -- as well as spatial periodicity with wavenumber k; thus

$$\tilde{\psi}(x,y,t) = \Psi(y,t) + \varepsilon\psi(x,y,t) \tag{A-4}$$

Substitution of (A-4) into (A-2) yields

$$(\nabla^2\Psi)_t - R^{-1}\nabla^4\Psi + \varepsilon[(\nabla^2\psi)_t + \Psi_y(\nabla^2\psi)_x - \psi_x(\nabla^2\Psi)_y - R^{-1}\nabla^4\psi] +$$
$$\varepsilon^2[\psi_y(\nabla^2\psi)_x - \psi_x(\nabla^2\psi)_y] = 0 \tag{A-5}$$

and upon x - averaging

$$(\nabla^2\Psi)_t - R^{-1}\nabla^4\Psi + \varepsilon^2 < \psi_y(\nabla^2\psi)_x - \psi_x(\nabla^2\psi)_y > = 0 \tag{A-6}$$

which is the equation governing the time evolution of the mean flow. The equation describing the evolution of the periodic disturbance follows readily upon subtraction of (A-6) from (A-5), viz

$$(\nabla^2\psi)_t + \Psi_y(\nabla^2\psi)_x - \psi_x(\nabla^2\Psi)_y - R^{-1}\nabla^4\psi +$$
$$\varepsilon[\psi_y(\nabla^2\psi)_x - \psi_x(\nabla^2\psi)_y - < \psi_y(\nabla^2\psi)_x - \psi_x(\nabla^2\psi)_y >] = 0 \tag{A-7}$$

Equation (A-6) indicates that, for $\varepsilon^2 > R^{-1}$, the mean flow vorticity $(\nabla^2\Psi)$ varies on a slow time scale $\tau = \varepsilon^2 t$, provided the disturbance stream function remains of order unity under differentiation with respect to the space coordinates. Under these conditions the solution of (A-7) may be sought by the method of multiple scales (e.g., Nayfeh 1973) and a uniform expansion for the disturbance stream function in powers of ε may be obtained according to

$$\varepsilon\psi(x,y,t) = \sum_{n=1}^{3} \varepsilon^n \psi_n(x,y,t,\tau) \tag{A-8}$$

With a single eigenmode excited at $t = 0$ the leading term of the solution (A-8) must have the form

$$\psi_1(x,y,t,\tau) = \frac{1}{2}[A_1(\tau)\ \zeta_1(y,\tau)\ e^{i\Theta} + c.c.] \tag{A-9}$$

where

$$\frac{\partial\Theta}{\partial x} = k \qquad \frac{\partial\Theta}{\partial t} = -\omega(k,\tau)$$

Substitution into (A-7) then shows that the function $\zeta_1(y,\tau)$ must satisfy the Orr-Sommerfeld equation

$$\mathcal{L}_1(\zeta_1) = (\zeta_{1yyyy} - 2k^2\zeta_{1yy} + k^4\zeta_1) -$$
$$iR[(Uk - \omega)(\zeta_{1yy} - k^2\zeta_1) - kU_{yy}\zeta_1] = 0 \qquad \text{(A-10)}$$

with the homogeneous boundary conditions

$$y = 0 \qquad \zeta_1 = \zeta_{1y} = 0 \qquad \text{(A-11a)}$$

$$y \to \infty \qquad \zeta_1 \to 0,\ \zeta_{1y} \to 0 \qquad \text{(A-11b)}$$

However, the function $A_1(\tau)$ remains undetermined at this level of approximation.

Further elaboration of (A-7) in the context of the solution (A-8) shows that the contribution ψ_2 to the disturbance stream function must have the form

$$\psi_2(x,y,t,\tau) = \frac{1}{4}\left[A_1^2(\tau)\ \zeta_2(y,\tau)\ e^{2i\Theta} + c.c.\right] \qquad \text{(A-12)}$$

the function $\zeta_2(y,\tau)$ being the solution of the equation

$$\mathcal{L}_2(\zeta_2) = (\zeta_{2yyyy} - 8k^2\zeta_{2yy} + 16k^4\zeta_2) -$$
$$2iR[(Uk - \omega)(\zeta_{2yy} - 4k^2\zeta_2) - kU_{yy}\zeta_2] =$$
$$-kiR(\zeta_1\zeta_{1yyy} - \zeta_{1y}\zeta_{1yy}) \qquad \text{(A-13)}$$

subject to the boundary conditions

$$y = 0 \qquad \zeta_2 = \zeta_{2y} = 0 \qquad \text{(A-14a)}$$

$$y \to \infty \qquad \zeta_2 \to 0,\ \zeta_{2y} \to 0 \qquad \text{(A-14b)}$$

The function $A_1(\tau)$ still remains undetermined.

An equation for $A_1(\tau)$ is obtained upon consideration of the contribution $O(\epsilon^3)$ to the solution (A-8). Elaboration of (A-7) to that order shows that the inhomogeneous part of the equation for ψ_3 includes, among others, terms proportional to exp $(i\Theta)$, which are contributed by the derivative of ψ_1 with respect to the slow time variable τ. Secular terms in the particular solution for ψ_3, and the attendant nonuniformity of the

expansion (A-8), can then be avoided only by seeking the particular solution in the form

$$\psi_3(x,y,t,\tau) = \frac{1}{2}\left[A_1(\tau)|A_1(\tau)|^2\zeta_3(y,\tau)e^{i\theta} + c.c.\right] \tag{A-15}$$

the function $\zeta_3(y,\tau)$ being the solution of the inhomogeneous equation

$$\mathcal{L}_1(\zeta_3) = R(A_1|A_1|^2)^{-1}\left[A_1(\zeta_{1_{yy}} - k^2\zeta_1)\right]_\tau -$$
$$\frac{iR}{4}\exp\left[i(\theta - \theta^*)\right]\left[k(2\zeta_2\,\zeta^*_{1_{yyy}} + \zeta_{2_y}\,\zeta^*_{1_{yy}}) -\right.$$
$$\left. 2k\zeta^*_{1_y}(\zeta_{2_{yy}} - 3k^2\zeta_2) - k\zeta^*_1(\zeta_{2_{yy}} - 3k^2\zeta_2)_y\right] \tag{A-16}$$

subject to the boundary conditions

$$y = 0 \qquad \zeta_3 = \zeta_{3_y} = 0 \tag{A-17a}$$

$$y \to \infty \qquad \zeta_3 \to 0,\ \zeta_{3_y} \to 0 \tag{A-17b}$$

In (A-16) $\mathcal{L}_1(\zeta_3)$ denotes the Orr-Sommerfeld differential operator -- defined by (A-10) -- and ζ^*_1 denotes the complex conjugate of ζ_1. The inhomogeneous problem consisting of equation (A-16) together with the boundary conditions (A-17a, b) then has a solution if, and only if, the inhomogeneous terms in (A-16) are orthogonal to every solution of the adjoint homogeneous problem. With (A-16) recast in the form

$$\mathcal{L}_1(\zeta_3) = i(A_1|A_1|^2)^{-1}\,(A_1 g_1)_\tau + \exp\left[i(\theta - \theta^*)\right]\,g_2 \tag{A-18}$$

where

$$g_1(y,\tau) = -iR(\zeta_{1_{yy}} - k^2\zeta_1) \tag{A-19a}$$

$$g_2(y,\tau) = -\frac{iRk}{4}\;2\zeta_2\zeta^*_{1_{yyy}} + \zeta_{2_y}\zeta^*_{1_{yy}} - 2\zeta^*_{1_y}(\zeta_{2_{yy}} - 3k^2\zeta_2) -$$
$$\zeta^*_1(\zeta_{2_{yy}} - 3k^2\zeta_2)_y \tag{A-19b}$$

we thus require that

$$\int_0^\infty \left\{(A_1 g_1)_\tau - iA_1|A_1|^2\exp\left[i(\theta - \theta^*)\right]\,g_2\right\}\tilde{\zeta}_1\,dy = 0 \tag{A-20}$$

$\tilde{\zeta}_1(y,\tau)$ being the eigenfunction that corresponds to the eigenvalue k of the adjoint homogeneous equation

$$\tilde{\mathcal{L}}(\tilde{\zeta}_1) = (\tilde{\zeta}_{1_{yyyy}} - 2k^2\tilde{\zeta}_{1_{yy}} + k^4\tilde{\zeta}_1) +$$
$$iR[(Uk - \omega)(\tilde{\zeta}_{1_{yy}} - k^2\tilde{\zeta}_1) + 2k/U_y\tilde{\zeta}_{1_y}] = 0 \tag{A-21}$$

subject to the boundary conditions

$$y = 0 \qquad \tilde{\zeta}_1 = \tilde{\zeta}_{1_y} = 0 \tag{A-22a}$$

$$y \to \infty \qquad \tilde{\zeta}_1 \to 0,\ \tilde{\zeta}_{1_y} \to 0 \tag{A-22b}$$

The condition (A-20) is readily recast into an ordinary differential equation for $A_1(\tau)$, namely

$$h_1(dA_1/d\tau) + h_2 A_1 + h_3 A_1 |A_1|^2 = 0 \tag{A-23}$$

where

$$h_1(k,\tau) = \int_o^\infty g_1 \tilde{\zeta}_1 \, dy \tag{A-24a}$$

$$h_2(k,\tau) = \int_o^\infty g_{1_\tau} \tilde{\zeta}_1 \, dy \tag{A-24b}$$

$$h_3(k,\tau) = -i \exp\left[i\,(\theta - \theta^*)\right] \int_o^\infty g_2 \tilde{\zeta}_1 \, dy \tag{A-24c}$$

If the vorticity distribution (g_1) associated with the wave has negligible dependence ($g_{1\tau}$) on the slow time τ we can set $h_2(\tau) = 0$ and solve (A-23) in closed form, viz

$$A = |A| \exp(-i|A|^2 \sigma_2 \tau) \tag{A-25}$$

with $\sigma_2 = -i\, h_3\, h_1^{-1}$. To a first approximation the wave motion is then described by

$$\psi(x,y,t) = \frac{1}{2}\left\{|A(\tau)|\ \zeta_1(y) \exp[i(\theta - \varepsilon^2|A|^2\sigma_2 t)] + c.c.\right\} \tag{A-26}$$

with obviously amplitude-dependent frequency

$$\omega + \varepsilon^2|A|^2\, \sigma_2 \tag{A-27}$$

The result clearly accomodates the experimental finding of Blackwelder and Kaplan (1976) that conditionally sampled velocity fluctuations display amplitude-independent signtures that propagate at amplitude-dependent velocities.

APPENDIX B

THE MODULATION OF A PACKET OF FINITE AMPLITUDE WAVES

For simplicity we consider a packet of two-dimensional finite amplitude waves that roughly approximate the features of Bark's (1975) results for the linear response $S_{uu}(k_x)$ of a turbulent boundary layer to a burst-associated Reynolds stress pulse (see Section 2.2 and Figure 2.2). We assume that the wave packet initially involves a dominant frequency ω_o -- associated with the wavenumber k_o at which S_{uu} peaks -- and two sidebands with frequencies $\omega_o \pm \nu$ and wavenumbers $k_o \pm \chi$. Since the peak of S_{uu} is quite narrow we set $\nu << \omega_o$ and $\chi << k_o$. As the waves possess finite amplitude and nearly coincident phase velocities (see Figure 2.5), we admit of significant nonlinear wave-wave interactions. Below we explore the consequences of those interactions upon the development of the spectrum; specifically, we seek to show that the interactions between the sidebands and the difference wave (of frequency ν and wavenumber χ) lead to amplitude and phase modulations of the dominant frequency ω_o.

In the presence of wave-wave interactions the amplitude a_n of the nth sideband -- with frequency $\omega_n = (\omega_o + n\nu)$ and wavenumber $k_n = (k_o + n\chi)$ evolves in time obeying the equation (see Kim, et al., 1980)

$$2i \frac{\partial a_n}{\partial t} = V_n^-(k_n,k_{n-1},\chi)\, a_{n-1}\, b \exp(i\Delta_n t) + V_n^+(k_n,k_{n+1},-\chi)\, a_{n+1}\, b^* \exp(-i\Delta_{n+1} t) \qquad \text{(B-1)}$$

where $V_n^-(V_n^+)$ denotes the coupling coefficient between the waves present at ω_n and $\omega_{n-1}(\omega_{n+1})$, b denotes the amplitude of the difference wave with frequency ν and wavenumber χ, and $\Delta_n = (\omega_n - \omega_{n-1} - \nu)$. As the difference wave arises as the result of nonlinear interactions among the original carrier and sidebands -- which are characterized by $(\partial\omega/\partial\alpha) \simeq (\omega/\alpha)$ -- we also have $(\nu/\chi) \simeq (\omega/\alpha)$ and, thus, $\Delta_n \simeq \Delta \simeq 0$. The coupling is then efficient and near-resonant among all the considered frequencies. Under those conditions (B-1) may be recast in the form

$$(d\tilde{a}_n/d\tau) = \frac{1}{2}\,(v_n^-\,\tilde{a}_{n-1} - v_n^+\,\tilde{a}_{n+1}) \tag{B-2}$$

with

$$\tilde{a}_n = a_n \exp\{in[\tfrac{\pi}{2} - \arg(b)]\} \tag{B-3a}$$

$$\tau = V_o \int_o^t |b|dt' \tag{B-3b}$$

$$v_n^- = (V_n^-/V_o), \quad v_n^+ = (V_n^+/V_o) \tag{B-3c}$$

Inspection of (B-2) indicates that, if the coupling coefficient is independent of n (i.e., $v_n^- = v_n^+ = 1$), the equation reduces to the recurrence relation among Bessel functions. The solution then is

$$\tilde{a}_n = J_n(\tau) \tag{B-4}$$

tantamount to a pure phase modulation of the dominant frequency ω with maximum frequency deviation $(\delta\omega_{max}/\nu) = \tau$. By contrast, if the coupling coefficient has a dependence on wavenumber, both amplitude and phase modulation ensue. The characteristics of these modulations can generally be determined by first integrating (B-2) to determine the amplitude of the nth sideband and then adding the sidebands to the carrier. The process may be carried out in closed form in the particular case where the coupling coefficient exhibits a slow variation with wavenumber such that

$$(v_n^-/v_n^+) = (1 - \delta)/(1 + \delta) \tag{B-5}$$

with $\delta << 1$; the result is [Kim, et al., 1980]

$$\sum_n a_n \exp[i(k_n x - \omega_n t)] + \text{c.c.} =$$

$$a(x,t)\cos[k_o x - \omega_o t + p(x,t)] \tag{B-6}$$

with

$$a(x,t) = 1 - \tau\delta \sin(\chi x - \nu t - \dot{\tau}) \qquad \text{(B-7a)}$$

$$p(x,t) = \tau \sin(\chi x - \nu t - \tau - \tfrac{\pi}{2}) \qquad \text{(B-7b)}$$

Rapid growth of the difference mode with consequent rapid development of the phase modulation index τ, defined by (B-3b) and exhibited in (B-7b), is expected for the waves excited by a TBL burst because of the near resonance between the dominant frequency ω_0 and the first sidebands that are also excited directly. The wavenumber dependence of the coupling coefficients, and the consequent magnitude of the amplitude modulation index $\tau\delta$ exhibited in (B-7a), are expected to be weak ($\delta << 1$) due to the lack of dispersion inherent to the nonlinear forcing of all other sideband modes. The nonlinear processes here considered then accommodate the theoretical proposition -- set forth in this report -- that the distinctly broad velocity fluctuation spectra measured by Morrison, et al., (1971) for $k \gtrsim k_0$, $\omega \gtrsim \omega_0$ result from a phase modulation of the narrower spectra which Bark (1975) calculates as the linear response of the turbulent boundary layer to the burst-associated Reynolds stress pulse.

REFERENCES

1. Bark, F.H., 1975, J. Fluid Mech., 70, 299-250.
2. Bergeron, R.F., Jr., 1973, J. Acoustic. Soc. Amer., 54, 123-133.
3. Blackwelder, R.F. and Kaplan, R.E., 1976, J. Fluid Mech., 76, 89-112.
4. Blackwelder, R.F. and Eckelmann, H., 1979, J. Fluid Mech., 94, 577-594.
5. Blake, W.K., 1970, J. Fluid Mech., 44, 637-660.
6. Blake, W.K. and Chase, D.M., 1971, J. Acoustic. Soc. Amer., 49, 862-877.
8. Corner, D. et al., 1976, J. Fluid Mech., 77, 81-103.
9. Crighton, D.G. and Gaster, M., 1976, J. Fluid Mech., 77, 397-413.
10. Dimotakis, P.E. and Brown, G.L., 1976, J. Fluid Mech., 78, 535-560.
11. Emmerling, R. et al., 1973, AGARD Conf. Noise Mechanisms Preprint No. 131.
12. Ffowcs Williams, J.E. and Kempton, A.J., 1978, J. Fluid Mech., 84, 673-694.
13. Fuchs, H.V. et al., 1979, J. Fluid Mech., 93, 185-207.
14. Grosch, C.E. and Salwen, H., 1978, J. Fluid Mech., 87, 33-54.
15. Gustavsson, L.H., 1979, Phys. Fluids, 22, 1602-1605.

16. Hatziavramidis, D.T. and Hanratty, T.J., 1979, J. Fluid Mech., 95, 655-679.

17. Jameson, P.W., 1975, Proceedings of the Symposium on Turbulence in Liquids, University of Missouri, Rolla, 192-200.

18. Khadra, L. et al., 1981, ASME Book No. H00201, Computers in Flow Predictions and Fluid Dynamics Experiments (Chia, K.N., Mueller, T.J. and Patel, B., Eds.)

19. Kim, H.T., Kline, S.J. and Reynolds, W.C., 1971, J. Fluid Mech., 50, 133-160.

20. Kim, Y.C. et al., 1980, Phys. Fluids, 23, 2250-2257.

21. Landahl, M.T., 1967, J. Fluid Mech., 29, 441-459.

22. Mack, L.M., 1976, J. Fluid Mech., 73, 497-520.

23. Maidanik, G. and Jorgensen, D.W., 1967, J. Acoust. Soc. Amer., 42, 494-501.

24. Martin, N.C. and Leehey, P., 1977, J. Sound Vibration, 52(1), 95-120.

25. Miksad, R.W. et al., 1982, Experiments on the Role of Amplitude and Phase Modulations During Transition to Turbulence. To appear in J. Fluid Mech.

26. Morrison, W.R.B. et al., 1971, J. Fluid Mech., 47, 639-656.

27. Nayfeh, A.H., 1973, Perturbation Methods, Wiley, New York, Chap. 6.

28. Phillips, O.M., 1956, Proc. R. Soc. London, 234, 327- .

29. Salwen, H. and Grosch, C.E., 1981, J. Fluid Mech., 104, 445-465.

30. Vaglio-Laurin, R. and Liu, N.S., 1981, New York University, DAS 81-06, (Submitted to J. Fluid Mech.).

31. Vaglio-Laurin, R., Hoglund, R.F. and Collier, R.D., 1982, ORI TR 2064.

32. Willmarth, W.W., 1975, Ann. Rev. Fluid Mech., 7, 13-38.

33. Yuen, H.C. and Ferguson, W.E., 1978, Phys. Fluids, 21, 1275-1278.